

The fingerprints of flexure in slab seismicity

Dan Sandiford*, Louis Moresi , Mike Sandiford, Rebecca Farrington, Ting Yang

*Corresponding author: dan.sandiford@utas.edu.au

This paper is a non peer reviewed pre-print submitted to AGU Tectonics

The fingerprints of flexure in slab seismicity

D. Sandiford^{1,2,3}, L.M Moresi^{2,4}, M. Sandiford², R. Farrington², T. Yang⁵

¹Institute of Marine and Antarctic Studies, University of Tasmania

²School of Earth Sciences, University of Melbourne

³Helmholtz Centre Potsdam - German Research Centre for Geosciences (GFZ)

⁴Australian National University

⁵Southern University of Science and Technology

Key Points:

- Intermediate depth seismicity is controlled by bending in a wide range of settings
- Geometric differences lead to contrasting seismic expression between east and west Pacific slabs
- Double seismic zones associated with bending are often masked by the strong temperature controls on seismicity

14 **Abstract**

15 East Pacific (ePac) slabs are characterised by downdip tension (DT) at intermediate depths,
 16 whereas most west Pacific (wPac) slabs are dominated by downdip compression (DC,
 17 e.g. Tonga) or have mixed mechanisms indicative of unbending (e.g. Kuriles). In this
 18 study we argue that despite these contrasts, flexural modes associated with slab bend-
 19 ing/unbending govern the seismic expression of slabs in both settings, thus challenging
 20 the prevailing paradigm that slab strain rates are dominated by uniform modes (stretch-
 21 ing or shortening). Firstly, we demonstrate that earthquake clusters consistent with slab
 22 unbending are present in ePac slabs, in addition to previously recognized wPac locations.
 23 A key difference is that unbending takes place at much shallower depths in ePac slabs,
 24 often ceasing at around 60 km, whereas unbending in wPac slabs can extend beyond 200
 25 km. We then show how systematic geometric differences between ePac and wPac slabs
 26 leads to additional zones of bending at intermediate depths in ePac slabs. The major-
 27 ity of ePac DT seismicity is clustered in curvature-increasing (+ve bending rate) zones
 28 associated with full or partial slab flattening. We argue that because seismicity is restricted
 29 to the colder parts of slabs at temperatures below about 600°C, typically only the ex-
 30 tensional upper part of these +ve bending rate zones are seismically active. Below the
 31 neutral plane, the corresponding shortening is mostly accommodated aseismically thereby
 32 masking the development of diagnostic polarized double seismic zones expected for flex-
 33 ural modes. We illustrate our hypothesis with results from a numerical subduction model
 34 in which geometry-controlled flexural modes dominate the slab deformation rate. While
 35 our framework is consistent with the notion that geometric controlled deformation dom-
 36 inates slab strain rates, we argue that the expression of slab buoyancy (e.g. slab pull)
 37 is discernible in terms of a systematic modifying effect on the seismic expression of flex-
 38 ure.

39 **1 Introduction**

40 Plate motions are driven primarily by density heterogeneities in the mantle. It is
 41 generally accepted that the most important density heterogeneities are associated with
 42 the oceanic plates where they sink into the mantle at subduction zones (Conrad & Lithgow-
 43 Bertelloni, 2002; Elsasser, 1969; McKenzie, 1969). Inclined zones of earthquakes beneath
 44 arcs delineate the geometry of these subducting slabs and provide a unique insight into
 45 slab dynamics. To the extent that rupture mechanisms of intermediate depth earthquakes

46 are thought to reflect, at least to some degree, the force balance in subducting slabs, they
 47 have been used to provide key insights into the basic mechanisms of plate tectonics. The
 48 force system in slabs include buoyancy forces due to thermal and metamorphic density
 49 contrasts, flexural stress associated with slab bending and unbending, and resistance arising
 50 from slip along the subduction interface and deeper mantle penetration (e.g. Fujita
 51 & Kanamori, 1981a; House & Jacob, 1982; Isacks & Molnar, 1971; Sleep, 1979).

52 Intermediate-depth earthquakes have traditionally been defined as those in the ~
 53 70-300 km depth range, where the subducting slab is detached from the over-riding plate
 54 (Gutenberg & Richter, 1954). The studies of (Isacks & Molnar, 1969, 1971) provided a
 55 number of enduring insights related to intermediate depth slab seismicity. They showed
 56 that the least/most extensive eigenvectors of earthquake moment tensors tend to be aligned
 57 in the slab downdip direction, consistent with the slab acting as a stress guide in a weaker
 58 mantle (Elsasser, 1969). They also identified that the co-seismic deformation patterns
 59 at intermediate depths correlate with broader seismic distribution in the slab. Slabs seg-
 60 ments with no deep earthquakes, or significant gaps between intermediate and deep earth-
 61 quakes, usually exhibit downdip tension/stretching (DT). (The notion of tension here
 62 refers to an effective rather than an absolute state of tension). In contrast, slabs with
 63 deep and continuous seismicity tend to be dominated by downdip compression/shortening
 64 (DC). Based on these spatial relationships, Isacks and Molnar (1971) helped to estab-
 65 lish the prevailing paradigm that slab earthquake orientations mainly reflect uniaxial,
 66 or uniform, stress/strain modes. To quote a recent study “slabs seem to be stretching
 67 as gravity acting on excess mass in the slabs pulls them down, like dangling springs hang-
 68 ing from and attached to lithosphere above” (Molnar & Bendick, 2019).

69 The correlations identified by Isacks and Molnar (1971) relate to the seismicity pat-
 70 terns in individual slab segments, yet they also expose contrasts in the seismic expres-
 71 sion between slabs along the eastern margin of the Pacific Ocean (ePac) and those along
 72 the western margin (wPac). In ePac slabs, intermediate depth focal mechanisms are strongly
 73 dominated by DT earthquakes. The Nazca slab in Chile is seen as archetypal ePac DT
 74 setting, which is often attributed to stretching due to slab pull (Bailey, Becker, & Ben-
 75 Zion, 2009; Bloch, Schurr, Kummerow, Salazar, & Shapiro, 2018; Isacks & Molnar, 1971;
 76 Rietbrock & Waldhauser, 2004). This contrasts most strikingly with wPac Pacific Plate
 77 subduction beneath Tonga, where intermediate depth focal mechanisms are dominated
 78 by DC events. DC regimes have been attributed to the propagation of compressional stress

79 along the slab from interactions between the deep parts of the slab and the transition
 80 zone (Billen, Gurnis, & Simons, 2003; Fujita & Kanamori, 1981b; Gurnis, Ritsema, Hei-
 81 jst, & Zhong, 2000).

82 The role of flexural deformation has mainly been discussed in relation to Pacific
 83 Plate subduction, e.g. northern Japan, Kuriles, Tonga, northern Marianas and eastern
 84 Aleutians. In these regions intermediate depth focal mechanisms exhibit a systematic
 85 polarity switch, suggesting that the upper part of the slab mantle is in downdip com-
 86 pression while the lower part is in down dip tension (Engdahl & Scholz, 1977; Hasegawa,
 87 Umino, & Takagi, 1978; Kawakatsu, 1986a, 1986b; Kita, Okada, Hasegawa, Nakajima,
 88 & Matsuzawa, 2010; Samowitz & Forsyth, 1981; Sleep, 1979; Tsukahara, 1980; Wang,
 89 2002). These Double Seismic Zones (DSZ) are consistent with unbending in the pres-
 90 ence of dehydration embrittlement. Other studies have noted regional correlations be-
 91 tween geometry (i.e. ‘warping’ or ‘flexure’) and seismicity, particularly in shallow slab
 92 settings (Craig & Copley, 2018; McCrory, Blair, Waldhauser, & Oppenheimer, 2012).

93 However, because some DSZs continue beyond the expected depths of unbending,
 94 and others have an opposite polarity to that expected from slab unbending (Comte et
 95 al., 1999), additional sources of stress have been argued to play a significant role in lo-
 96 calising DSZ seismicity (Brudzinski, Thurber, Hacker, & Engdahl, 2007; Fujita & Kanamori,
 97 1981b). Other studies have focused on DSZs as a metamorphic/dehydration phenom-
 98 ena, without explicit consideration of the contribution the stress field in which they nu-
 99 cleate (Peacock, 2001). Indeed, while metamorphic and fluid processes have long been
 100 seen as necessary ingredient for intermediate depth nucleation (e.g. Isacks & Molnar, 1971),
 101 this metamorphic framework has come to dominate discussions of slab seismicity in re-
 102 cent decades (Chen, Manea, Niu, Wei, & Kiser, 2019; Faccenda, 2014; Green & Hous-
 103 ton, 1995; Hacker, Peacock, Abers, & Holloway, 2003; Kirby, Engdahl, & Denlinger, 2013;
 104 Peacock, 2001; Seno & Yamanaka, 2013; Tsujimori, Sisson, Liou, Harlow, & Sorensen,
 105 2006).

106 Even allowing for the strong weakening role played by dehydration, the concept that
 107 some slabs undergo appreciable rates of stretching (10^{-15} s^{-1} , (e.g. Kawakatsu, 1986a))
 108 implies high deviatoric stresses. This is because uniform stretching involves not only the
 109 brittle deformation of weakened (e.g. fluid-overpressured) crust and mantle, but also de-
 110 formation of the deeper, ductile slab core (e.g. F. A. Capitanio, Morra, & Goes, 2009).

111 Conrad and Lithgow-Bertelloni (2004) argued that effective tensional stress magnitudes
 112 may be as much as 500 MPa, in order to produce bulk stretching rates in the order of
 113 10^{-15} s $^{-1}$, assuming effective slab viscosity several hundred times higher than a typi-
 114 cal upper mantle value. While uncertainties in slab rheology mean such high stress es-
 115 timates are speculative, these magnitudes lie in the range of plausible estimates, given
 116 that the thermal and compositional buoyancy forces in subducting slabs are of order 10^{13}
 117 N.m $^{-1}$.

118 In this study we argue that flexural modes accompanying slab bending and unbend-
 119 ing provide an important control on the seismic moment release in many Pacific mar-
 120 gin slab segments, but in ways that are subtly obscured by thermal controls. We show,
 121 firstly, that earthquakes due to slab unbending are much more widespread than previ-
 122 ously recognised, occurring in both ePac and wPac slabs. An important difference be-
 123 tween ePac and wPac slabs is that unbending takes place at much shallower depth in the
 124 former. Hence, most ePac unbending earthquakes have strong spatial overlap with the
 125 megathrust zone, and so have been largely overlooked in previous analyses. In section
 126 3 we describe a procedure to filter megathrust earthquakes from global catalogs, that helps
 127 reveal this characteristic ePac signature of shallow unbending.

128 We then show how systematic geometric complexities lead to additional zones of
 129 bending in ePac slabs, that are absent in wPac slabs. The majority of ePac DT seismic-
 130 ity is conspicuously clustered in curvature-increasing zones associated with full or par-
 131 tial slab flattening. In such zones, we speculate that seismicity is mainly restricted to
 132 the cold, upper half of the slabs, where they evidence down-dip stretching and that the
 133 associated shortening in the lower half of the slab is largely accommodated aseismically.
 134 Crucially, while the larger earthquakes, as found in the global CMT catalog, have uni-
 135 form DT seismicity in Chile, microseismic studies have revealed an oppositely-polarised
 136 DSZs (Comte & Suarez, 1994), consistent with the model presented here. The frame-
 137 work implies that strain rates associated geometric bending/unbending rates are larger
 138 than those associated uniform stretching modes due to, for example, slab pull. This is
 139 consistent with the notion that slab buoyancy is largely supported by drag in the up-
 140 per mantle.

141 **Notes on terminology**

142 In this section we clarify the terminology we use in discussing seismicity and slab
 143 dynamics. Intermediate-depth earthquakes are traditionally defined as those lying in the
 144 70-300 km depth range \sim 70-300 km depth range. As we will show, the somewhat ar-
 145 bitrary restriction to events deeper than about 70 kms has imposed some important lim-
 146 itations. We will use term ‘slab’ or ‘intralab’ earthquakes to refer to all earthquakes in
 147 the subducting lithosphere: that is, from the onset of bending of the plate (tradition-
 148 ally called outer-rise earthquakes) to the deepest limit of seismicity (\sim 700 km). How-
 149 ever, our analysis focuses only on earthquakes shallow than 300 km. The reasons for this
 150 restriction are: 1) constraints on slab geometry and accuracy of earthquake hypocenters
 151 are likely to decrease with greater depth; 2) the global distribution of slab earthquakes
 152 shows a local minimum at around 300 km depth (e.g. Vassiliou, Hager, & Raefsky, 1984).
 153 On the other hand, our analysis assumes no intrinsic distinction between earthquakes
 154 above and below 70 km. We will still occasionally refer to intermediate depths, as this
 155 remains a valid (and familiar) specification of a particular depth range.

156 The term outer-rise earthquakes is potentially a misnomer, because earthquakes
 157 that result from curvature increase of the incoming plate are limited not only to the outer
 158 rise, but in some slabs extends landward of the trench, beneath the shallow part of the
 159 fore-arc. Hence we will refer to the region where the incoming plate experiences increas-
 160 ing curvature as ‘outer bending zone’ (or OBZ). Downdip of the OBZ, after passing through
 161 peak curvature, slabs invariably straighten in a zone of unbending which we term the
 162 primary unbending zone (or PUZ).

163 In discussing contributions to the slab deformation rate, we emphasise the distinc-
 164 tion between uniform modes and flexural/bending modes. We use the terms flexure and
 165 bending somewhat interchangeably, in keeping with historical developments in the lit-
 166 erature. Flexural strain (rates) is associated with changes in curvature. Curvature is con-
 167 sidered positive when the plate/slab is concave down, which means that the slab hinge
 168 in typical subduction zones has positive curvature. For reasons that will be discussed
 169 in more detail, our analysis makes the assumption that strain (rates) associated with bend-
 170 ing is two-dimensional (related to changes in curvature in the downdip direction). Strain
 171 rates due to flexural deformation are characterised by an anti-symmetry across the neu-
 172 tral plane. The polarity depends on the sign of the bending rate: positive bending rates,

173 where where curvature is increasing, are associated with downdip extension above the
 174 neutral plane and downdip compression below. Arguments that slab seismicity is con-
 175 trolled by bending/unbending, are based on the identification of an analogous polarity
 176 switch in earthquake moment tensors. In referring to ‘uniform’ modes of deformation,
 177 we mean either bulk slab stretching or shortening in the downdip direction. The prevail-
 178 ing paradigm for slab seismicity emphasises uniform deformation modes, particularly in
 179 connection with ePac DT zones (e.g. Isacks & Molnar, 1971).

180 It is important to note that our use of the term flexure is essentially divorced from
 181 the context of elastic sheet mechanics, where the term flexure is also very common. If
 182 slabs behaved as competent elastic sheets, we would expect that stress would vary sys-
 183 tematically with the total curvature, and in the process of unbending the plate would
 184 simply return to an undisturbed elastic state. An important conclusion of our study (re-
 185 inforcing a range of previous arguments) is that the instantaneous elastic strain contri-
 186 bution in slabs is a relatively minor component of the total flexural deformation.

187 2 Data

188 2.1 Slab geometry and region selection

189 In this study we consider ePac slab segments in Chile, Peru and Central America,
 190 and wPac slab segments in Tonga, Japan (northern Honshu) and the Kuriles. The seis-
 191 mic expression of these regions is described in Section 4. An important component of
 192 our analysis involves correlations between measures of downdip slab geometry (e.g. cur-
 193 vature gradient) and the seismic expression. A convenient way of assessing these rela-
 194 tionships is by using regional sections across the subduction system, in which patterns
 195 of aggregated seismicity (trench parallel) can be compared to the characteristic slab ge-
 196 ometry.

197 In choosing regions suitable for analysis, a balance is sought between slab segments
 198 that encompass sufficient well constrained slab earthquakes, while also having a relatively
 199 strong morphological similarity along strike. The complicating issue, which we discuss
 200 later in more detail, is that the greater the along-strike distance, the more variability in
 201 morphology, the very effects of which we are seeking to isolate.

202 Using either the Slab1 and Slab2 models (Hayes et al., 2018; Hayes, Wald, & John-
 203 son, 2012) we construct regionally-averaged slab surface profiles. We begin by interpo-

204 lating the chosen slab model along a series of trench perpendicular lines spaced at ap-
 205 proximately 10 km intervals along the trench. The azimuth of these lines is shown in the
 206 region maps (e.g Fig. 3). Because the slab models do not always extend to the trench,
 207 we build a spline representation between the regionally-averaged slab model profile and
 208 bathymetry data from ETOPO1 (Amante & Eakins, 2009), thus providing a continu-
 209 ous representation of the slab model that extends well into the surface oceanic plate. We
 210 then average these individual profiles to generate a single representative slab surface ge-
 211 ometry that provides a consistent fit to the earthquake hypocenters at intermediate depths.

212 Like earthquake hypocenters, the 3D morphology of slabs in the upper mantle is
 213 subject to uncertainty, particularly in regions where seismicity is sparse and/or slab mor-
 214 phology is inherently complex. The recent Slab2 surface model (Hayes et al., 2018) uses
 215 multiple input data types to augment earthquake-derived slab geometry models. The
 216 use of multiple input data sources in the Slab2 model is likely to improve the overall ac-
 217 curacy of the subduction geometry, however in doing so it appears to sacrifice consistency
 218 with earthquake hypocenter data in some locations. This problem is particularly evident
 219 in Tonga, where the Slab2 model clearly deviates from the earthquake hypocenters at
 220 intermediate depths (see Fig. 6). In general, we find the Slab1 model to be more con-
 221 sistent with the global ISC-EHB earthquake catalog for slabs in the wPac (Tonga, Japan
 222 Kuriles). However, the Slab2 model covers the ePac slabs in significantly more detail than
 223 Slab1. In particular, the Slab2 model seems to better capture the extent of slab flatten-
 224 ing in Peru and partial slab flattening in Chile, relative to the older Slab1 model (for ex-
 225 ample, as shown in Fig. 9). This partial flattening of the northern Chile slab is well con-
 226 strained by earthquake hypocenters as has been discussed in a number of previous stud-
 227 ies Engdahl, van der Hilst, and Buland (1998); Fujita and Kanamori (1981b); Sippl, Schurr,
 228 Asch, and Kummerow (2018), and is important to our analysis.

229 In examining the relationships between between slab dynamics and geometry, we
 230 will refer frequently to the slab midplane. We use this term in relation to both the nu-
 231 matical model and observed slab geometries. The notion of a midplane serves as a proxy
 232 for the neutral plane of bending, and hence provides a way of analysing slab dynamics
 233 in terms of thin viscous sheet relationships (which are discussed in Section 5). Of course,
 234 the actual neutral plane of bending is a dynamic feature which may vary with respect
 235 to a fixed reference position such as the slab surface. However, for our purposes, knowl-
 236 edge of such variability is not essential. The analysis of the numerical model in Section

5, which is based on a slab surface referenced midplane, shows this approximation to the neutral plane is sufficient for understanding the key relationships between geometry and slab deformation rate. We generate a midplane by an orthogonal translation of the slab surface model, with a distance that is proportional to thermal thickness of the plate at the trench. We use a constant of proportionality of 0.2, consistent with estimates of how DSZ width increases with plate age (Brudzinski et al., 2007). The resulting slab midplane is illustrated in cross sections with dashed black lines (e.g. Fig. 6). Our analysis requires knowledge of the slab geometry and its downdip gradients. In estimating the curvature and curvature gradient of the midplane, a second order Butterworth filter is used to remove short wavelengths of less than about 100 km.

2.2 Earthquake data

The accuracy of teleseismic-determined hypocenters varies considerably with location technique, seismograph distribution, and hypocenter depth (e.g. Craig, 2019; Engdahl et al., 1998; Jackson, 1980). The approach we take to integrating available global earthquake datasets is informed by several factors: 1) if only teleseismic P and S wave travel times are used, depth errors may be several tens of km, due to fact that the origin time of an earthquake trades off against its focal depth (Jackson, 1980); 2) the use of depth phases means that depth uncertainty can be reduced to around 10-15 km, similar to epicentral uncertainties (Engdahl et al., 1998); 3) for shallow earthquakes (< 50 km), where the depth phases overlap with P wave coda, agency-reported depth phases are likely to be less accurate (Engdahl et al., 1998); 4) depth errors in the CMT database can be significantly higher than the best available global travel time data (Craig, 2019).

A simple way of addressing these issues is to combine the comprehensive CMT moment tensor database (Ekström, Nettles, & Dziewoński, 2012) with the hypocenters from the ISC-EHB database. The ISC-EHB location procedure uses depth phases, via the EHB algorithm (Engdahl et al., 1998), to minimise uncertainties in depth. In this study we only consider the subset of events that are contained in both the CMT and ISC-EHB catalogs, using moment tensor data from the former and hypocenter information from the latter. Completeness magnitudes for the combined dataset will be limited by CMT catalogue, which contains fewer small earthquakes than ISC-EHB. From 1976 - 2004 the CMT catalog was complete to 5.4, while in the period following 2004 this was reduced to Mw 5.0 (Ekström et al., 2012).

269 **3 Methods**

270 **3.1 Megathrust event filter methodology**

271 Earthquakes on the subduction megathrust constitute a very significant proportion
 272 of the overall seismic activity in shallow part of subduction zones. Although megathrust
 273 seismicity does not overlap spatially with intermediate depth earthquakes *sensu stricto*
 274 (> 70 km), filtering of potential megathrust events is extremely important in terms of
 275 identifying intraslab seismicity at shallow depths beneath the fore-arc wedge. Even with
 276 improved ISC-EHB locations, the depth uncertainties mean the use of hypocenter loca-
 277 tion data alone does not allow unambiguous discrimination of megathrust and intraslab
 278 events. Below we outline a procedure that combines both a seismic moment tensor sim-
 279 ilarity and hypocenter location to filter megathrust events from intraslab events.

280 We use the trench azimuth to define the strike and rake of the reference megath-
 281 rust rupture tensor (\mathbf{M}^{ref}), assuming a pure double-couple mechanism, with the slab dip
 282 is set to 20° close to the average observed dip beneath the fore-arc in the regions con-
 283 sidered here. The similarity measure (χ) of a given earthquake with (\mathbf{M}^k) is measured
 284 using the tensor dot product (:) of the normalised moment tensors:

$$\chi = \left[\frac{\mathbf{M}_{ij}^{\text{ref}} : \mathbf{M}_{ij}^k}{|\mathbf{M}^{\text{ref}}| |\mathbf{M}^k|} \right] \quad (1)$$

285 We assume an event is a megathrust rupture if it has a recorded depth is less than
 286 70 km, the hypocenter lies within 20 km of the Slab2 surface model and the moment ten-
 287 sor exhibits strong similarity to a reference megathrust rupture along the local part of
 288 the trench. We identify megathrust events using a focal mechanism similarity condition
 289 of $\chi \geq 0.75$. Fig. 1 show results from the application of this procedure along the Chile
 290 subduction zone. We focus in this region because it allows comparison with the recent
 291 publication of waveform-constrained hypocenters (Craig (2019), referred to here as Craig19).
 292 We note that the Craig19 data spans a shorter time interval than the ISC-EHB cata-
 293 log, and is limited in its spatial extent, which means that the union of the CMT events
 294 and the Craig19 hypocenters yields a much smaller dataset than the union of CMT and
 295 ISC-EHB. Fig 1 shows the T-axes of identified as megathrust ruptures (black/grey) and
 296 intraslab events (orange). The T-axes are represented as projections of a uniform length
 297 vector onto a vertical great-circle plane. The identified megathrust events define a set

298 of nearly-parallel T-axes, with the highest density of hypocenters being between 15 and
 299 40 km depth.

300 Because the majority of shallow subduction events in the catalog identify as megath-
 301 rust events in this procedure (see Fig. 2d), even a relative small set of misidentified events
 302 could induce biases in our analysis. Our procedure could lead to such misidentification
 303 if there are a significant number of megathrust events with atypical rupture, or if there
 304 are significant numbers of proximal intraslab earthquakes with ruptures that are sim-
 305 ilar to our reference megathrust source. To further assess this possibility, Fig. 2 shows
 306 statistical distributions for spatial and source-related features of the data in Chile. The
 307 histogram in Fig. 2d shows the value of the normalised tensor similarity and emphasises
 308 that the majority of events show a high correlation with the expected slip on a megath-
 309 rust, with the largest bin being the highest similarity. This does not rule out the pos-
 310 sibility that we may exclude some megathrust events with atypical rupture mechanisms,
 311 it suggests that the basic assumption about homogeneity of megathrust sources is valid.
 312 Moreover, Fig. 2d shows that the chosen similarity value of 0.75 is meaningful in terms
 313 of distribution of earthquake orientation, as it represents the transition from the rela-
 314 tively flat part of the histogram, to the region where the histogram rises steeply at high
 315 moment tensor similarity associated with megathrust ruptures.

316 Fig. 2a shows the T-axes of the CMT moment tensor in a slab surface (Slab2) ref-
 317 erence frame (as usual based on the ISC-EHB hypocenters). The vertical axis shows the
 318 distance of the earthquake hypocenter to the slab surface, while the horizontal axis shows
 319 distance along the slab surface. Histograms show the depth distribution (relative to the
 320 slab surface) for the two earthquake groups (i.e., megathrust and intraslab) shown in Fig.
 321 1. The rotated T-axes of megathrust earthquake identified in our procedure share a char-
 322 acteristic orientation, plunging landward at close to 45° relative to the slab (Fig. 2a).
 323 The spatial distribution of identified megathrust events has a mean very close to zero
 324 (as shown with horizontal solid black line) and a standard deviation of about 6.5 km.
 325 The normal distribution corresponding to the same mean and standard deviation val-
 326 ues is shown with black dashed lines in Fig 2a. The distribution is consistent with the
 327 idea that the typical maximum depth errors value have a value of 10 - 15 km (Engdahl
 328 et al., 1998). In practice we use a window of 20 km to capture megathrust events towards
 329 the tail of the distribution, which is important because of unequal population sizes (i.e.
 330 numbers of megathrust versus slab events). The distribution of identified megathrust earth-

quake is close to symmetric around the mean, consistent with the expected errors inherent in depth-origin time trade off, although a slightly larger number of megathrust group events lie in the lower half of the spatial window than in the upper half (Fig. 2a). This may indicate misidentification of some intraslab events. The orange histogram reflects the spatial distribution of events identified as intraslab earthquakes relative to the slab surface (only events shallower than 70 km are shown). The mean of these events is shown with the solid orange line, and lies at about 10 km below the slab surface. The distribution of the slab earthquakes is weakly bimodal, with a peaks at around 8 km and 20 km consistent with existence of a DSZ.

Fig 2c shows the same filtering applied to hypocenters in the Craig19 study. In this case, the events identified as megathrust ruptures are more compactly distributed, with a standard deviation of 4.6 km. As noted in (Craig, 2019), the mean of the megathrust events is systematically shallower than the Slab2 surface, by around 5km. Three identified megathrust events shown in Fig 2c lie more than 10 km from the mean value of the set, and may represent slab earthquakes with megathrust-like rupture mechanisms. As with the ISC-EHB data there a bimodal depth distribution for the intraslab group, with peaks at similar spacing, although deeper by a few kilometres, compared to the ISC-EHB data. Fig 2b compares the depth estimate for candidate megathrust events listed in both ISC-EHB and Craig19 after subtracting the mean value of the offset relative to the slab surface. The resulting difference in the depths between the 2 catalogs is up to 18 km, similar to the window width used (20 km) to identify potential megathrust events.

In addition to filtering megathrust events, all events with hypocentral depths more than 20 km above the Slab2 surface are assumed to be upper plate events and are excluded from our analysis. While this is consistent with the inferred depth error distribution for shallow earthquakes, it allows that some shallow forearc events may be erroneously identified as intraslab earthquakes. We think that the inclusion of forearc events is relatively minor issue in most regions considered here. The interval post-Tohoku earthquake (2011) in Japan is an exception which we discuss specifically.

3.2 Numerical model

In Section 5 we discuss results from a numerical subduction model. The model was developed using the Underworld2 code, and is closely based on setup described in D. San-

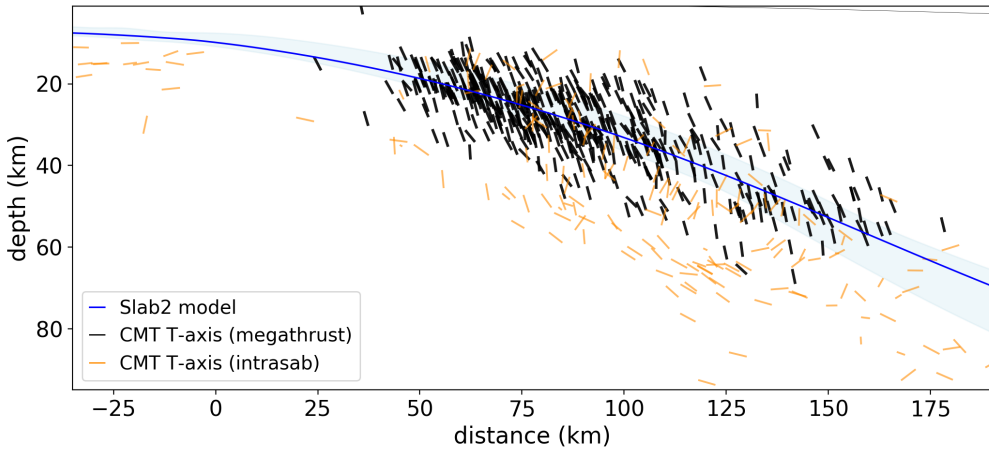


Figure 1. Distribution of filtered earthquakes in the near-trench zone (< 180 kms) in the Chilean region (Fig. 9 shows region bounds). Vectors represent CMT moment tensor T-axes, separated into inferred megathrust (black) and intraslab (yellow) events based on the similarity-procedure described in the main text. Hypocenters from the ISC-EHB Bulletin. Blue line shows the region-averaged Slab2 surface profile, while blue shaded region represents the variation of the Slab2 surface across the region.

362 diford and Moresi (2019). We refer readers to that study for a description of the gov-
 363 erning equations, numerical method, model rheology, and implementation of the subduc-
 364 tion interface. There are two significant changes in the setup of model described here:
 365 1) we use a larger domain, with a higher relative resolution; 2) we constrain the upper
 366 viscosity limit in a small part of the mantle wedge to a value of 2×10^{20} Pas. The ge-
 367 ometry of the viscosity-limited region is shown in Fig. A.1 and constitutes an extremely
 368 simplified attempt to account for processes such as the presence of volatiles and melts
 369 in the wedge which are expected to substantially reduce the effective viscosity compared
 370 to dry, melt-free conditions. In terms of the model evolution the viscosity limit applied
 371 to this region has the primary effect of allowing asymmetric subduction to proceed even
 372 when the slab dip angle becomes quite shallow. If we did not provide this upper limit
 373 on the viscosity, the shallow part of mantle wedge would increase in viscosity as the slab
 374 dip decreases, due to a reduction in temperature (e.g. England & Wilkins, 2004). This
 375 creates increased coupling with the upper plate, and a rapid feedback cycle that results
 376 in a breakdown of single-sided subduction in model simulations.

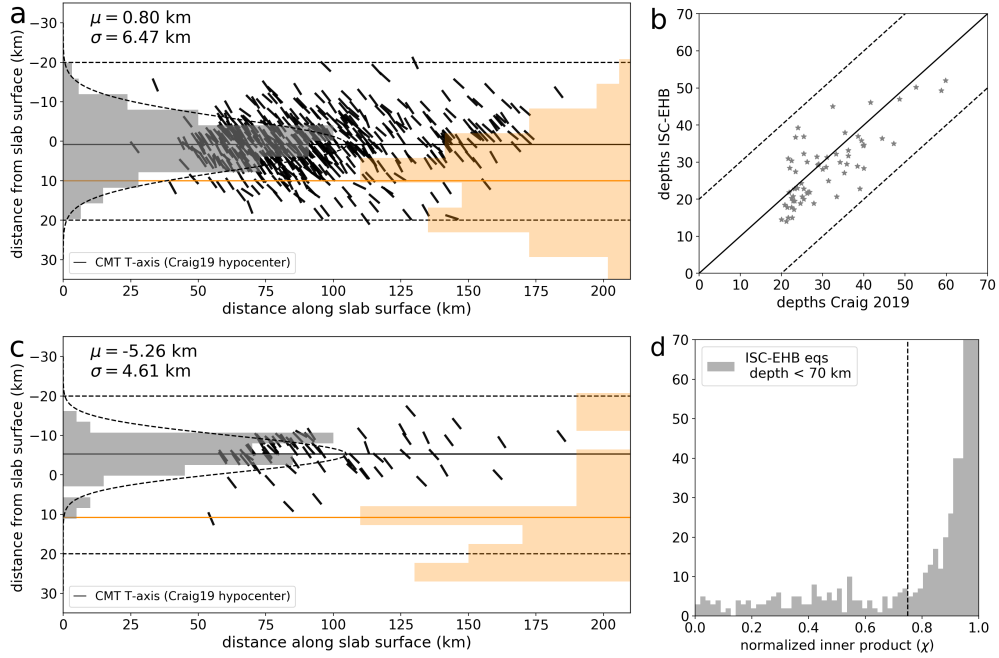


Figure 2. Statistical attributes of filtered earthquake locations in the near-trench zone for Chile region (see Fig. 9). a) CMT T-axes rotated into a slab-surface coordinate system, where the vertical axis is the distance from the slab surface, and the horizontal coordinate is the distance along the slab surface, relative to the location of the trench. Histograms show the distribution of the distance of the hypocenter (ISC-EHB) to the slab surface for megathrust events (grey) and intraslab events (yellow). Solid horizontal lines show the mean of the distribution; c) as for above, with hypocenters taken instead from the catalog of Craig19 (Craig, 2019); b) comparison of depths for identified megathrust events that appear in both the ISC-EHB and Craig19 catalogs; d) Histogram shows the distribution of the moment tensor similarity (χ) for all events with depths less than 70 km. A similarity of $\chi = 1$ implies the moment tensor is identical to the reference megathrust event. Vertical dashed line shows the limiting similarity value ($\chi = 0.75$) used in to filter megathrust events.

377 Fig. 15 shows a schematic of the model domain, including the initial conditions,
 378 boundary conditions, and evolution of the slab morphology during the simulation. Ad-
 379 ditional information about the numerical model setup is contained in Appendix A.

380 4 Study regions and seismicity

381 4.1 Western Pacific (wPac) seismicity

382 We consider three wPac slab segments: Tonga, Japan (northern Honshu), and the
 383 Kuriles. The domain limits are shown in Figs. 3, 4 and 5, along with cross sections pro-
 384 viding a regional overview of slab seismicity. We have included deep (> 300 km) seis-
 385 micity in these images, although our analysis is restricted to earthquakes shallower than
 386 300 km. The coloured points show earthquakes designated as intraslab events. Earth-
 387 quakes that lie more than 20 km above the slab surface (in the slab normal direction)
 388 are shown as small black points in the domain overview figures (e.g. Fig. 3). This step
 389 in our processing is primarily intended to capture upper plate events, which we there-
 390 fore exclude from our analysis. However because we have not limited this condition in
 391 terms of absolute depth, we also capture a small number of slab earthquakes. Such anom-
 392alous earthquake locations may indicate substantial outliers in the data, or places where
 393 the region-averaged slab model does not adequately capture local irregularities in slab
 394 morphology at depth. Because the along-strike morphology of slabs tends to become more
 395 variable with depth, the deviation in hypocenters from the model slab geometry also tends
 396 to increase with depth. This accounts, for instance, for the large number of outliers in
 397 Tonga at depths > 300 km. Importantly, however, the region-averaged slab surface ge-
 398ometries provide a generally consistent fit to slab seismicity in wPac slabs at depths less
 399 than 300 km.

400 In Figs. 6-8 we highlight the orientation of slab earthquake moment tensors in the
 401 wPac slabs. The T-axes of the CMT moment tensors are plotted as projected vectors
 402 onto trench-perpendicular vertical planes (plane azimuths are shown on the region maps,
 403 e.g. Fig. 3). The length variation in the plotted T-axes reflects the magnitude of the pro-
 404 jected component of the vector. That most of the T-Axes in the figures tend to have a
 405 similar length is a reflection that the least/most extensive eigenvectors of earthquake mo-
 406 ment tensors tend to point downdip in slabs (Isacks & Molnar, 1971). The T-axes are
 407 expected to lie within the same quadrant as the smallest stress eigenvector. A common

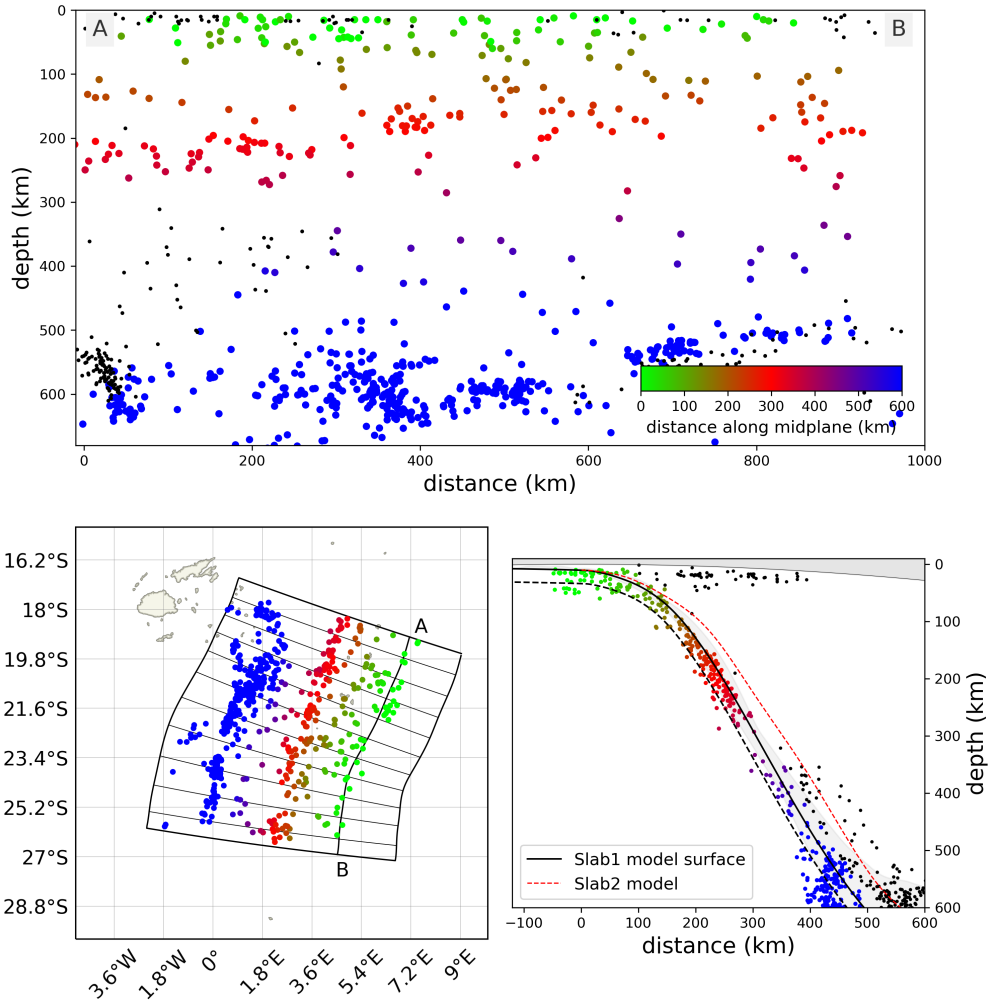


Figure 3. Overview of Tonga slab analysis region. Colored points show intraslab seismicity which is consistent with best available slab geometry model (Slab1 is used for Tonga region). Earthquakes lying more than 20 km above the slab surface are shown as small black points. We don't include these events in our analysis, as they can either be considered upper-plate events, outliers (presumably due to depth error), or regions where our slab models do not properly resolve the local slab morphology. Earthquakes identified as likely megathrust ruptures are excluded in these figures. The upper panel shows earthquakes projected on a great-circle plane lying parallel to the trench at the mid-point of the domain. Lower-left figure shows slab earthquakes in map view. Lower-right panel shows projection of the earthquakes on a trench-parallel cross section: the solid black line shows the region-averaged slab surface model; the gray region shows the variation in slab surface across the domain; the dashed black line shows the slab midplane (an orthogonal translation of the slab surface, as discussed in the main text); the red dashed line shows the Slab2 model for Tonga, which shows much less consistency with the earthquake hypocenters (ISC-EHB catalog).

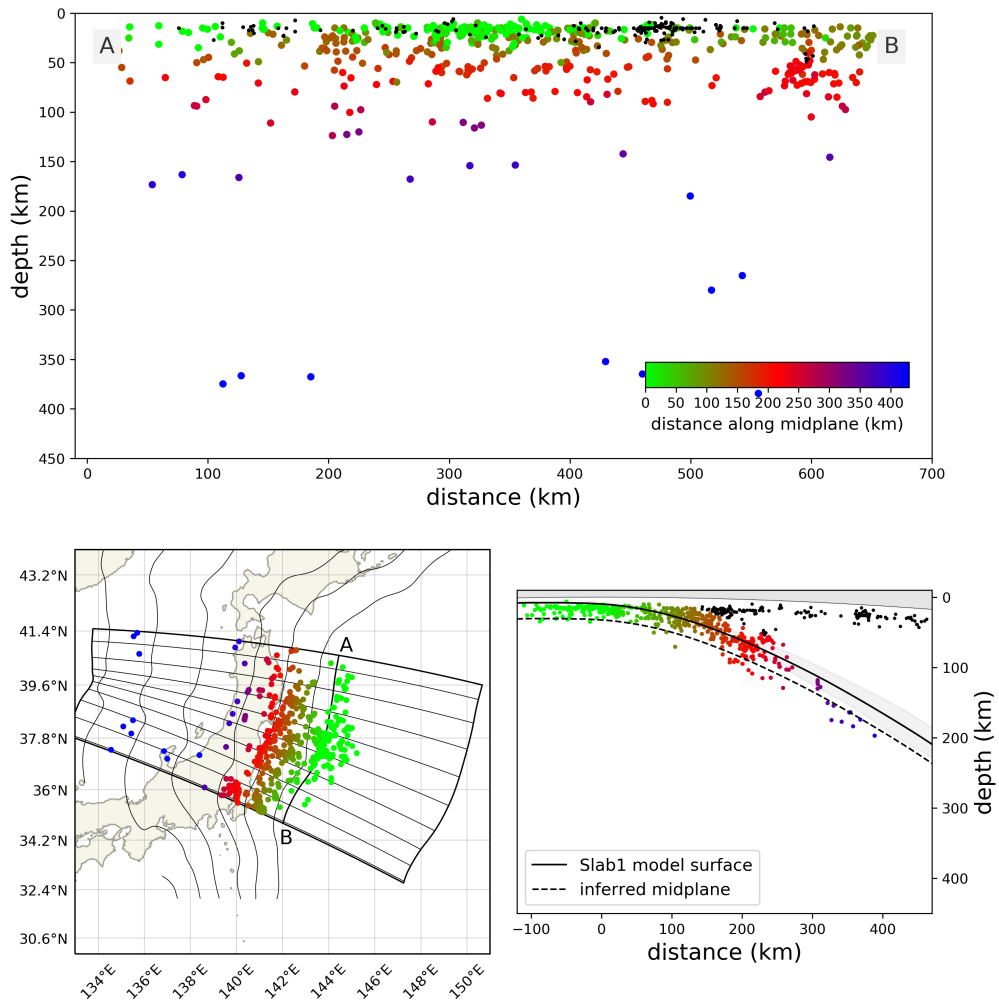


Figure 4. Overview of Japan slab analysis region. See Fig. 3 caption for details of figure organisation and preparation.

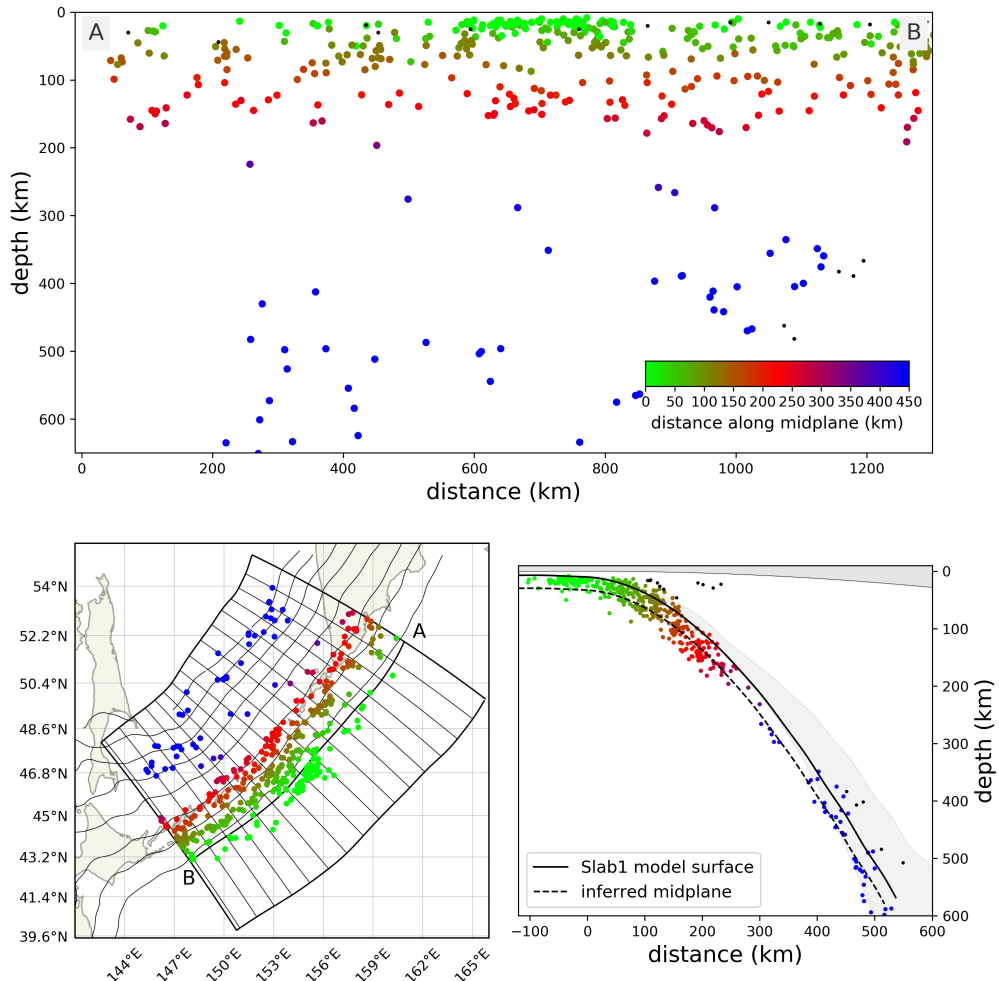


Figure 5. Overview of Kuriles slab analysis region. See Fig. 3 caption for details of figure organisation and preparation.

408 interpretation is that T-axes represent the orientation of most extensive co-seismic strain
 409 release (Bailey et al., 2009; Isacks & Molnar, 1971; Yang, Gurnis, & Zhan, 2017). The
 410 color of the T-axes represents the angle relative to the local slab orientation. Red axes
 411 show earthquakes with a DC sense, and blue axes those with a DT sense.

412 Outer Bending Zone (OBZ) events are evident in all wPac slab settings, typically
 413 starting at a distance between 50-120 km outboard of the trench. The fact that bend-
 414 ing contributes to the stress-state in the outer-rise region is relatively uncontroversial (Chap-
 415 ple & Forsyth, 1979; Craig, Copley, & Jackson, 2014). In the wPac slab regions consid-
 416 ered here, OBZ earthquakes cluster outboard of the peak in slab curvature which occurs
 417 landward of the trench (see also Figs. 17-19 and discussion in Section 6).

418 Historically, the role of unbending in slab seismicity has mainly been investigated
 419 in relation to Pacific Plate subduction (i.e. Kuriles, Japan, Tonga, Aleutians, and north-
 420 ern Marianas) (Engdahl & Scholz, 1977; Hasegawa et al., 1978; Kawakatsu, 1986a, 1986b;
 421 Samowitz & Forsyth, 1981; Tsukahara, 1980; Wang, 2002). The key observation is that
 422 these regions have DSZs which exhibit a characteristic ‘polarity’ switch in moment ten-
 423 sor between the upper and lower bands, characterised by DC and DT events, respectively.
 424 This distribution is very clear in the Kurile slab (Fig. 8) where a clear offset in the lo-
 425 cus of DC and DT events occurs at depths between 70 - 200 km. The focal mechanism
 426 polarity switch, which is the defining feature of unbending-related DSZs, is also evident
 427 in both the Tonga and Japan slabs, although in both cases the relative number of lower
 428 plane DT to upper plane DC events is lower than in the Kuriles (e.g. Kawakatsu, 1986b).
 429 Importantly, while the PUZ in both Tonga and Japan is dominated by DC events, nei-
 430 ther are exclusively DC (Figs. 6-8). As we discuss further below this is contrary to the
 431 expectation of uniform slab shortening of previous analyses (e.g. Fujita & Kanamori, 1981b;
 432 Isacks & Molnar, 1971; Richter, 1979).

433 At depths of around 60 - 200 km in the Japan slab, we see a clear indication of a
 434 polarised DSZ. Compared to the seismicity in the Kuriles and Tonga, the PUZ seismic-
 435 ity in the Japan slab is somewhat more clustered, particularly with regard to the dis-
 436 tribution of lower plane DT events. We note that the great Tohoku megathrust event
 437 in 2011 impacted the Japan subduction zone during the catalog interval considered here.
 438 A result of the Tohoku earthquake is the appearance of a large cluster of extensional earth-
 439 quakes in the shallow part of forearc (as labelled in Fig. 7), as discussed in previous stud-

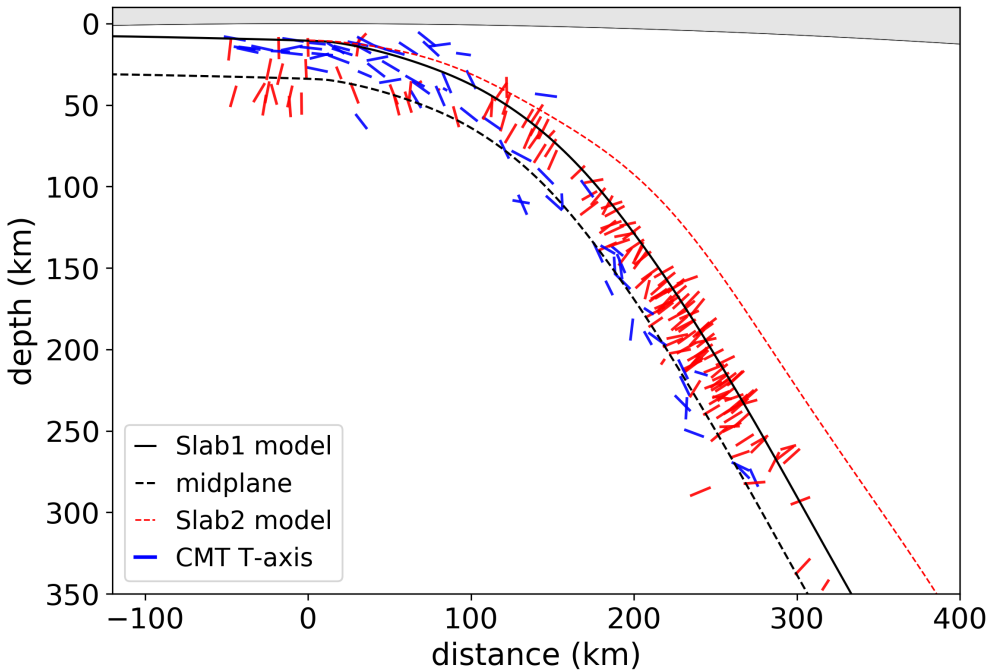


Figure 6. Tongan slab profile section. Projection of CMT T-axes (ISC-EHB hypocenters) on a vertical cross-section, along the azimuths shown with dashed lines in Fig. 3, with data aggregated across the entire domain. The T-axes are plotted as projections of uniform-length vectors, with the length variation in the plotted T-axes reflecting the magnitude of the projected component of the vector. T-axes are coloured according to the orientation relative to the slab midplane (shown with dashed black line): red represents earthquakes with a DC sense, blue with a DT sense.

ies (Imanishi, Ando, & Kuwahara, 2012). These events mainly lie within the 20 km window used to filter upper plate events, and are therefore misidentified as DT slab earthquakes. Supplementary Fig. B.1 shows the earthquakes in the catalog prior to 2011, where the shallow forearc events are much fewer. The Tohoku earthquake also appears to have influenced aspects of the intraslab earthquake distribution. For instance, a comparison of Fig. 7) and Fig. B.1 suggests that unusually high levels of OBZ earthquakes have occurred in the ~ 8 yrs since Tohoku. Interestingly, it appears that the number of unbending (PUZ) events in the has not increased in a comparable way, suggesting that stress changes associated with the megathrust rupture have not influenced the deeper parts of the slab as significantly as the incoming plate.

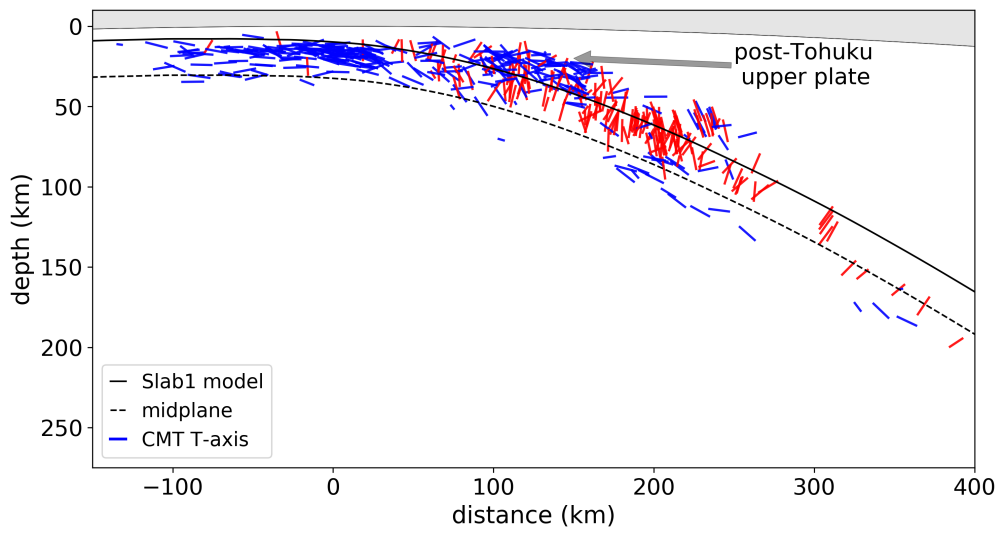


Figure 7. Japanese slab profile section. See Fig. 6 caption for details of figure organisation and preparation.

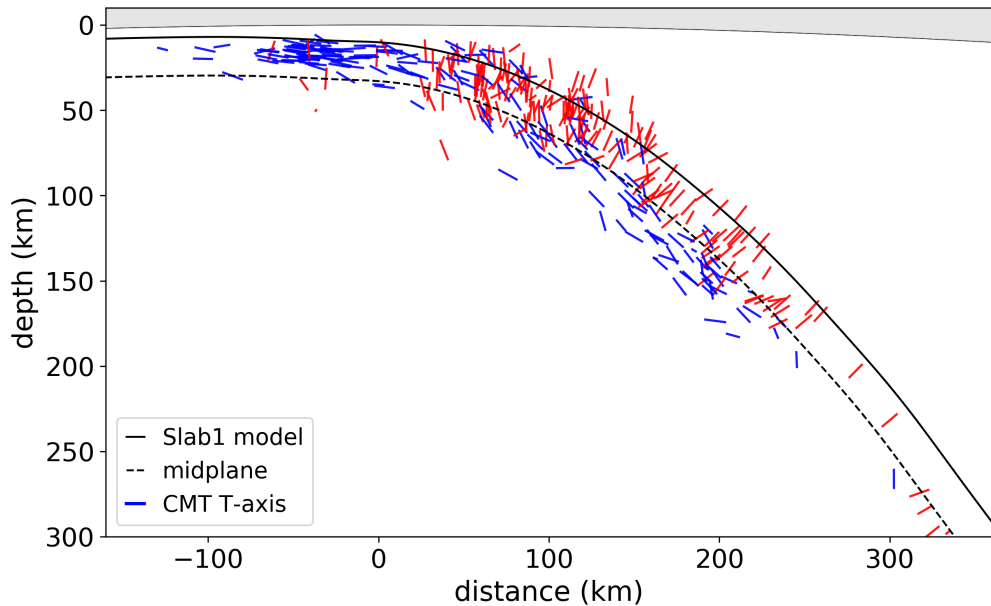


Figure 8. Kuriles slab profile section. See Fig. 6 caption for details of figure organisation and preparation.

450 **4.2 Eastern Pacific (ePac) seismicity**

451 Along the ePac margin we consider slab segments in Chile, Peru and Central Amer-
 452 ica. The location of the regions are shown in Figs. 9 - 11, along with cross sections pro-
 453 viding a regional overview of slab seismicity. As we have already discussed, the along-
 454 strike morphology of the ePac at intermediate depths slabs shows a greater degree of vari-
 455 ability than is typical of wPac slabs. The presence of a number of prominent flat slab
 456 segments, such as Chile (Pampean), Peru and Mexico, is a reflective of this variability.
 457 This means that in addition to the ubiquitous presence of both OBZ and PUZ, ePac slabs
 458 commonly exhibit additional zones of bending and unbending.

459 Due to relatively low rates of seismicity OBZ and PUZ, resolving the seismic ex-
 460 pression in the ePac slabs requires aggregating earthquakes across a significant distance
 461 along slab strike (~ 1000 km). Because the slab morphology is relatively coherent at these
 462 shallow depths, the analysis of aggregated earthquakes (and slab geometry) in the OBZ
 463 and PUZ is straightforward. However, with increasing downdip distance this coherence
 464 degrades. One implication is that a single ‘region averaged’ slab geometry is less capa-
 465 ble of representing full variation in slab morphology, along with the range of seismicity
 466 contained therein. These issues are most significant in the case of Chile, which warrants
 467 some further discussion.

468 The Chile region, shown in Fig. 9, extends from the Bolivian Orocline in the north,
 469 to south of the Pampean flat slab. Within this region significant variation in slab mor-
 470 phology occurs, mainly associated with the Pampean flat slab, where the Juan Fernan-
 471 dez ridge subducts. Despite this variability, we treat the entire region as single domain.
 472 This takes advantage of the fact that: a) the width of the Pampean flat slab is relatively
 473 narrow with respect to the size of the domain, and b) the rates of intermediate depth
 474 seismicity in the Pampean slab very are low compared to the northern part of the Chile
 475 slab (i.e. the north Chile seismic belt, shown in Fig. 9). Because of the skewed nature
 476 of seismic activity, the main contribution to the aggregated intermediate depth seismic-
 477 ity (i.e. when plotted in cross section) comes from northern Chile. Of course, if we were
 478 only interested in immediate depth seismicity (> 70 km), it would suffice to simply con-
 479 sider restricted region in the northern part of the domain. This would mean, however,
 480 that the seismic expression of the OBZ and PUZ would be less clearly defined. Hence,
 481 the cross section for Chile (Fig. 12) provides something of a dual perspective: with the

shallow seismicity (< 70 km) being reflective of region-wide seismic expression, while the intermediate depth seismicity is dominated by the north Chile seismic belt. Because the main contribution to the intermediate depth seismicity in Chile comes from the north Chile Seismic Belt, our geometric analysis (section 6) is based on a slab surface model that reflects the slab morphology in north.

OBZ earthquakes are evident in all ePac slab settings, reflected in normal faulting events in the upper part of lithosphere. When compared to the wPac settings discussed above, two differences stand out. In ePac the frequency of OBZ events is significantly lower, and the OBZ events tend to be clustered much closer to the trench. In Peru, the small number of OBZ events are all located within about 10 kms of the trench, with most of these in fact being slightly landward (Fig. 13).

Clusters of earthquakes at about 100 km inboard of the trench in Chile, and 150 km in Peru, provide evidence for the existence of unbending DSZs along the ePac margin (Figs. 12 - 13, see also Figs. 20 - 21 as discussed in Section 6). Both cases contain a band of dominantly DC events overlying a smaller group of DT events. As we will show in Section 6, these events occur in the region where inferred rates of slab unbending are highest (i.e. in the PUZ). Compared to the wPac, an important difference in the PUZ seismic expression is the relative depths at which they appear. Because the ePac unbending events occur at relatively shallow depths and spatially overlap with the megathrust zone, removing of the megathrust event is critical to their resolution. While the significance of ePac DC events in terms of a putative unbending DSZ, have been noted previously (e.g. Barazangi & Isacks, 1976) this interpretation has not previously gained much traction, and other studies have posited alternative interpretations, such as slab-push (Lemoine, Madariaga, & Campos, 2002), or flexural slip (Romeo & Álvarez-Gómez, 2018).

Downdip from the PUZ, the slab morphology in Chile and Peru deviates substantially. Peru has a very long (~ 300 km) flat slab region, followed by a steepening associated with a prominent peak in curvature at around 600 km from the trench (the distal hinge of the flat slab section). The trench normal view of Peruvian seismicity, shown in the upper panel of Fig. 10 is striking. Earthquakes in the flat slab form a belt, with an average depth of ~120 km, over a distance extending more than 700 km along the trench, with a slight concave up distribution. A cluster of earthquakes, known as the Pucallpa seismic nest, forms a subset of these flat slab earthquakes, and are proximal to

514 a localised depression along the distal hinge of flat slab (Gutscher, Spakman, Bijwaard,
 515 & Engdahl, 2000; Wagner & Okal, 2019). Our regionally averaged slab morphology clearly
 516 does not captures this subtle variation. In Fig. 13 the Pucallpa events have been high-
 517 lighted using a greater transparency level.

518 While the slab morphology for northern Chile, shown in Fig. 12, does not contain
 519 a prominent flat slab *sensu stricto*, there is a subtle upwards deflection beginning at around
 520 200 km from the trench indicative of partial flattening. While the profile section shows
 521 this as a subtle feature, the implied curvature is quite sharp, as discussed further below.

522 In both Chile and Peru, slab seismicity at intermediate depths is dominated by DT
 523 ruptures. In Peru, seismicity is distributed throughout the flat slab, becoming more fre-
 524 quent towards the distal hinge. In Chile, the DT events evident in Fig. 12 are clustered
 525 in two zones. The first of these overlaps with the zone of partial slab flattening, between
 526 200 and 350 kms from the trench, centered at a depth of ~ 110 km, and appear as red
 527 points in Fig. 9. The second cluster is more diffuse, concentrated between 400 and 500
 528 km from the trench, appearing as blue points in Fig. 9. When viewed in a trench-parallel
 529 cross section (Fig. 9 upper panel), the two zones of intermediate depth DT seismicity
 530 in Chile have quite different characteristics. This shallower zone forms a sub-horizontal
 531 band of seismicity, which is most intense in the northern part of the domain (labelleled
 532 the ‘north Chile seismic belt’) but is also evident in parts of the southern half of the do-
 533 main. The deeper zone of DT seismicity has hypocenters which form a band oriented
 534 at a relatively high angle to a horizontal plane (i.e. Fig. 9 upper panel). We have high-
 535 lighted these earthquakes with a red dipping dashed line in Fig. 9. The framework pre-
 536 sented in this study has applicability to the north Chile seismic belt, but not the deeper
 537 earthquakes. The unusual distribution of this deeper cluster of earthquakes may indi-
 538 cate a spatially and temporally localised process like slab tearing, whereas our study at-
 539 tempts to highlight the signal of time-independent, geometric bending.

540 The patterns of seismicity in Central American slab are far less clear than the other
 541 regions we consider in this study. For instance, the hypocenter locations shown in the
 542 cross section (Fig. 14) exhibit substantial scatter at all depths, as well as less pronounced
 543 downdip clustering than in Chile or Peru (where we argue that such clusters are asso-
 544 ciated with different bending zones). One possibility is that the morphological variabil-
 545 ity of the Central America slab, even at shallow depths, blurs the patterns in the aggre-

546 gated seismicity. In the Central American region, the case for a seismicity associated with
 547 a PUZ is not clear. While there are a number of events in the Central American slab which
 548 have a DC component (red axes in Fig. 14), and could potentially indicate unbending,
 549 there is no clear spatial separation between DC events and the more numerous DT earth-
 550 quakes. Moreover, Fig. 14 shows that the principal-axes of the DC events, are not strictly
 551 aligned with the slab as is expected for unbending. It is possible that these DC events
 552 (red axes in Fig. 14) are deep, poorly located, megathrust ruptures, that have been misiden-
 553 tified in our filtering procedure.

554 The morphology of the slab in Central America is characterized by two distinct zones
 555 of steeping (based on the Slab2 geometry shown in Fig. 14). The slab unbends fully at
 556 about 100 km from the trench, before steepening again with a second peak in curvature
 557 at about 175 km from the trench. Unlike the other ePac settings we have discussed, no
 558 clear dip angle reduction takes place between these peaks in curvature. The majority of
 559 earthquakes in the Central American slab have DT ruptures, and are concentrated at
 560 a distance of about 130 km from the trench. As we show in Section 6, this places the ma-
 561 jority of DT earthquakes in a zone of curvature increase where, similar to the outer rise,
 562 stretching of the upper part of the slab is expected. We must highlight, however, that
 563 the consistency between the seismicity and the slab surface model is relatively poor in
 564 Central America, and we therefore place less emphasis on results from this region.

565 5 Insights from numerical modeling

566 In this section we present results from a numerical subduction model, which serves
 567 primarily to highlight how different modes contribute to the overall slab deformation rate.
 568 The setup of the numerical model is very similar to the description in D. Sandiford and
 569 Moresi (2019), and more extensive details of the model are provided in Appendix 1. The
 570 flow is driven entirely by the thermal density contrast of the slab. Mantle rheology (in-
 571 cluding oceanic lithosphere) is prescribed by a composite flow law that includes linear
 572 high-temperature creep, as well as a scalar visco-plastic approach sufficient for captur-
 573 ing psuedo-brittle as well as distributed plastic deformation within the slab (see A for
 574 additional information). The model does not include any stored elastic stress component.
 575 This common simplification assumes that elastic stress is relaxed on a relatively short
 576 time/length scales.

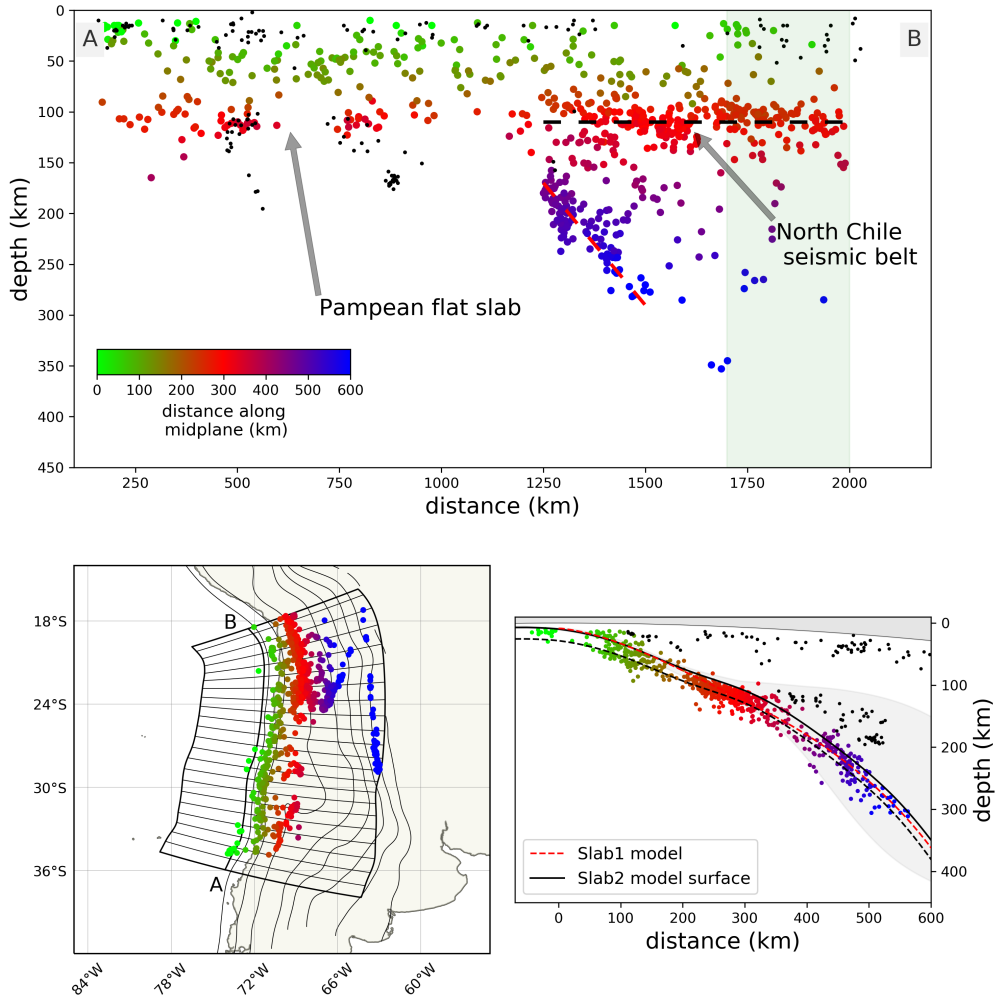


Figure 9. Overview of Chilean slab analysis region. See Fig. 3 caption for details of figure organisation and preparation. The black points represent earthquakes that lie more than 20 km above the slab surface model. These mainly represent the relatively small number of earthquakes that occur in close proximity to the Pampean flat slab in the south, where the slab morphology is quite different to northern Chile. The green band in the top panel corresponds to a restricted region which we plot in Fig. B.2.

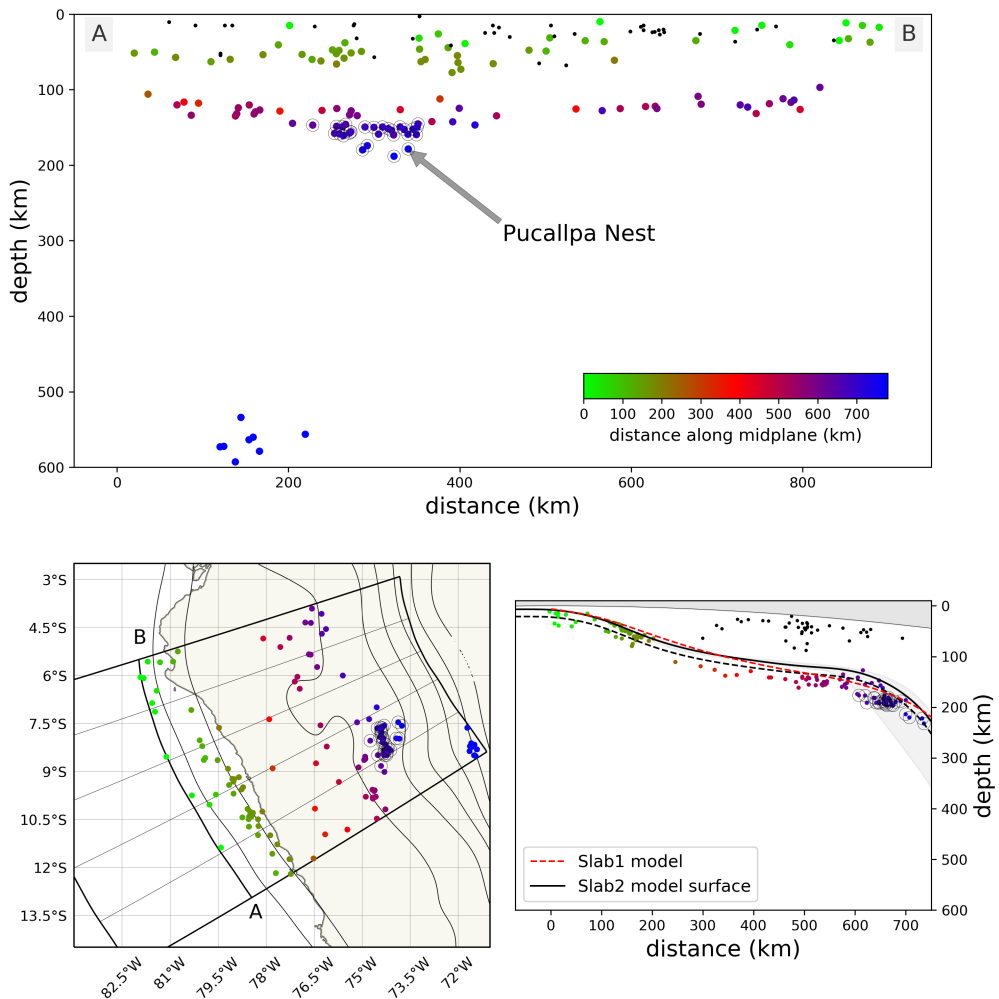


Figure 10. Overview of Peruvian slab analysis region. See Fig. 3 caption for details of figure organisation and preparation.

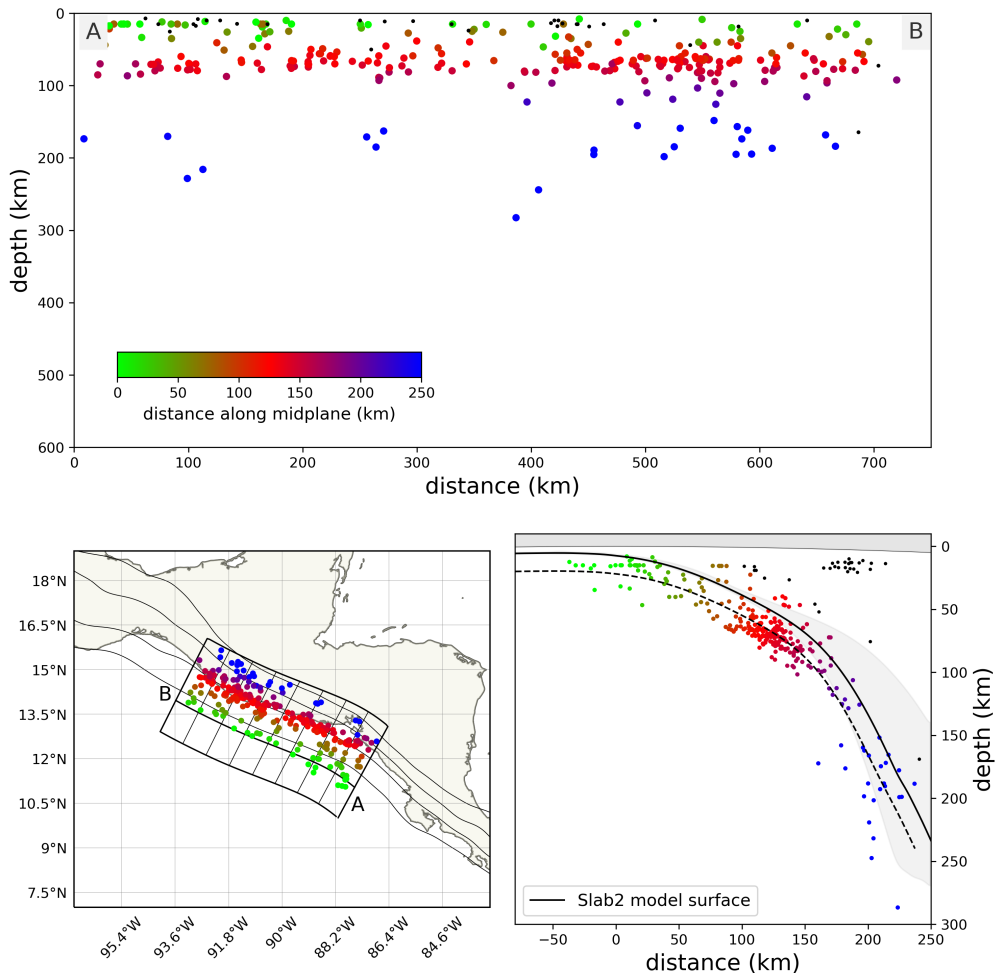


Figure 11. Overview of Central American slab analysis region. See Fig. 3 caption for details of figure organisation and preparation.

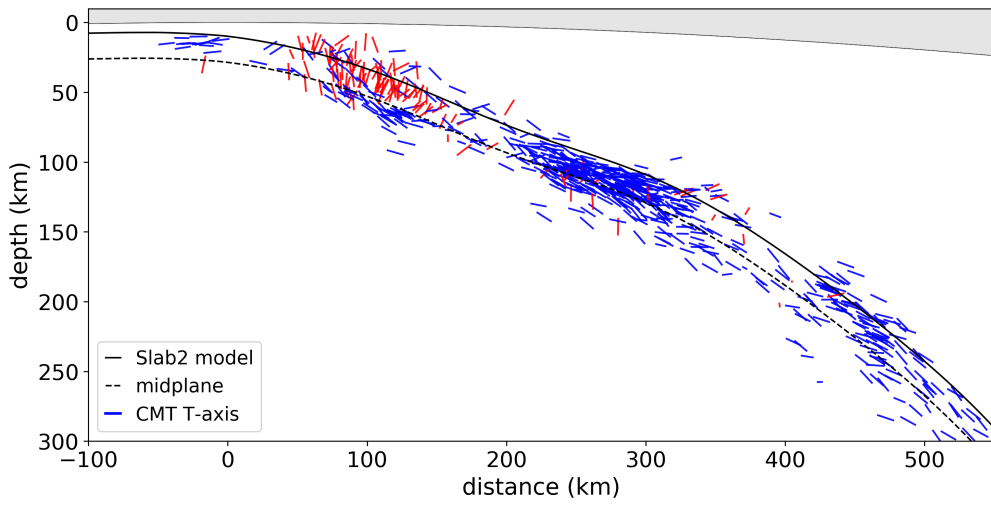


Figure 12. Chilean slab profile section. See Fig. 6 caption for details of figure organisation and preparation.

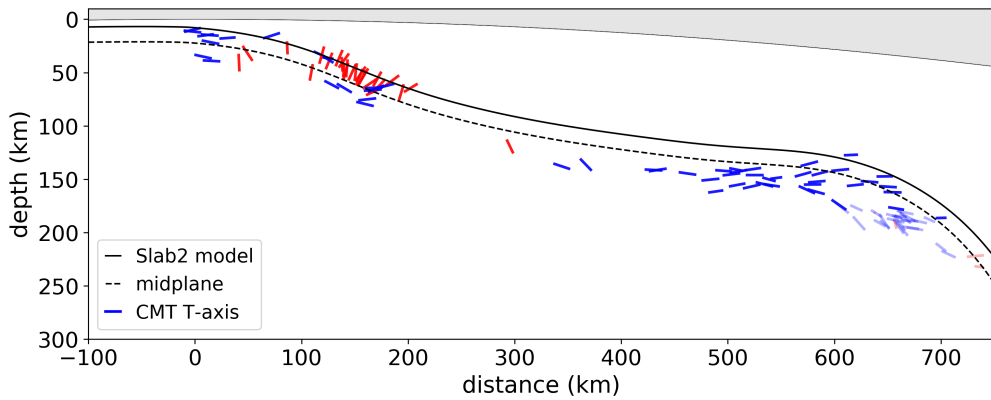


Figure 13. Peruvian slab profile section. See Fig. 6 caption for details of figure organisation and preparation.

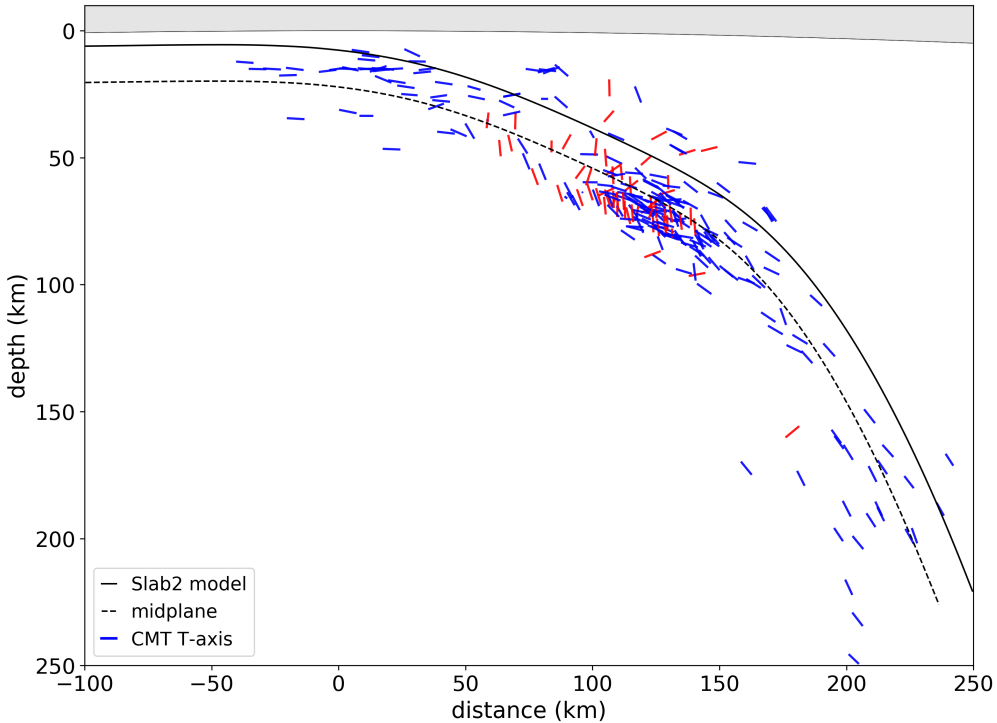


Figure 14. Central American slab profile section. See Fig. 6 caption for details of figure organisation and preparation.

In Fig. 16 we show the downdip component of the strain rate ($\dot{\epsilon}_{ss}$) at two time intervals, with the top panels in each figure showing the normalised value of curvature and curvature gradient evaluated along the slab midplane. The fact that flexural deformation dominates the downdip slab strain rate is apparent from observing that all regions of high strain rate are polarised, with shortening (red) on one side of the slab and stretching (blue) on the other. If uniform deformation modes were dominant, we would expect to see entire sections of slab undergoing stretching or shortening. It may seem surprising that a system which is driven entirely by slab buoyancy is not dominated by uniform stretching due to slab pull. This outcome is a consequence of the fact that nearly all of the slab pull force is balanced by drag in the mantle. This subduction style is often referred to as the Stokes regime (F. Capitanio, Morra, & Goes, 2007; Gerardi & Ribe, 2018; W. P. Schellart, 2004). In the inset axis of Fig. 16, at 10 Myr, we plot the stress in the subducting plate. The peak stress is on the order of 10 MPa. This is more than order of magnitude smaller than the stress that would be produced if a significant part of the

591 weight of the slab was connected to the plate (i.e. when the slab pull factor are *sim* 0.5(e.g.
 592 Conrad & Lithgow-Bertelloni, 2004)).

593 The numerical model shows that flexural, rather than uniform deformation modes,
 594 tend to dominate the subduction hinge in the Stokes regime. Another important insight
 595 provided by the model relates to the strong geometric control on bending rates. When
 596 a sheet is deformed by pure bending, the distribution of strain rate in the downdip di-
 597 rection ($\dot{\epsilon}_{ss}$) is a function of the curvature rate (a material derivative) multiplied by dis-
 598 tance from the midplane (Kawakatsu, 1986a; Ribe, 2001; Tsukahara, 1980):

$$\dot{\epsilon}_{ss} = -y \frac{DK}{Dt} = -y \left(\frac{\partial K}{\partial t} + u_s \frac{\partial K}{\partial s} \right) \quad (2)$$

599 where s refers to a unit vector along the slab midplane, y is the distance perpendicular
 600 to the midplane, $\frac{D}{Dt}$ is the material derivative following s , K is the curvature and u_s is
 601 the velocity component parallel to the midplane. The term $u_s \frac{\partial K}{\partial s}$ is sometimes referred
 602 to as an advective bending rate; we will also use the term geometric bending to empha-
 603 sise the the fact that it is the present day slab geometry that constrains this (time-independent)
 604 component of the bending rates.

605 At both of the time intervals shown in the Fig. 16, we see a strong correlation be-
 606 tween the curvature gradient profile ($\frac{\partial K}{\partial s}$) and the downdip strain rate distribution ($\dot{\epsilon}_{ss}$).
 607 The zones where downdip strain rates are smallest coincide with the local maxima in the
 608 curvature amplitude, where the curvature gradient is close to zero. This suggests that
 609 the advective component of the bending rate is a dominant control on the both the to-
 610 tal bending rate (as well as as the overall slab deformation rate). At 10 Myr, we see a
 611 typical slab morphology, characterised by plate bending outboard of the trench (OBZ)
 612 and slab unbending centered at around 70 km depth (PUZ). At 25 Myr, the slab has be-
 613 gin to deflect upwards beneath the upper plate. This zone is associated with increasing
 614 curvature (positive curvature gradient) which produces extension in the upper half the
 615 slab and shortening in the lower half of the slab. The numerical model morphology at
 616 25 Myr is reminiscent of the partial flattening of the Nazca slab in northern Chile (Fig.
 617 12).

618 The distribution of slab temperature, relative to patterns of internal slab dynam-
 619 ics, are important for thinking about which parts of the slab are likely to be seismogenic.
 620 The brittle ductile transition in lithospheric mantle is thought to occur at a potential

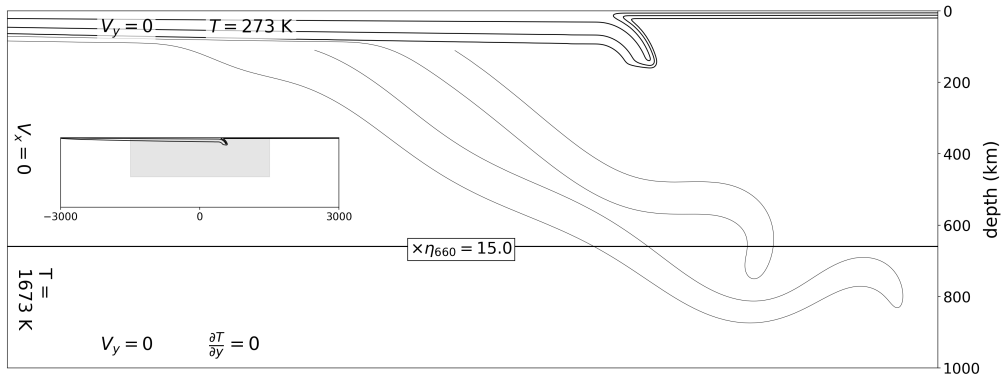


Figure 15. Numerical model setup. The main panel shows a restricted part of computational domain. Contours of the slab temperature show the evolution of the model at times 0, 10, 25 Myr. Inset panel shows the full computational domain (6000 km x 1500 km).

temperature near 600 °C (Emmerson & McKenzie, 2007). In the model, a gradual reduction in subduction velocity between 10 Myr and 25 Myr is a primary control on why the depth of the 600 °C isotherm has reduced from about 300 km to less than 150 km over that time interval. We note that in the numerical model, the 600 °C isotherm encloses the upper-half of each bending region: the simple prediction would be that strain would only be released seismically in the upper half of the bending zones (i.e. above the neutral plane). In many of slab we discussed regions, however, we see the seismic expression of both halves of the bending region, even if that distribution is often asymmetric. This points to a limitation in the subduction models, which should be kept in mind.

6 Seismicity geometry relationships

In this section we assess the role of advective bending in relation to the seismic expression of Pacific margin slabs. Within each slab region, the relative variation in the advective bending rate is associated with downdip curvature gradient of the neutral plane, according to the relationship in equation 2. We calculate curvature gradient using the estimated slab midplane (a proxy for the neutral plane) as described in Section 2. The visualisations we use to explore these seismicity geometry relationships differ somewhat to those in Section 4. Here we plot the earthquake T-axes in a slab midplane coordinate system, with distance from the hypocenter to the midplane shown on the vertical axis, and distance along the midplane relative to the trench (horizontal axes). As in the ear-

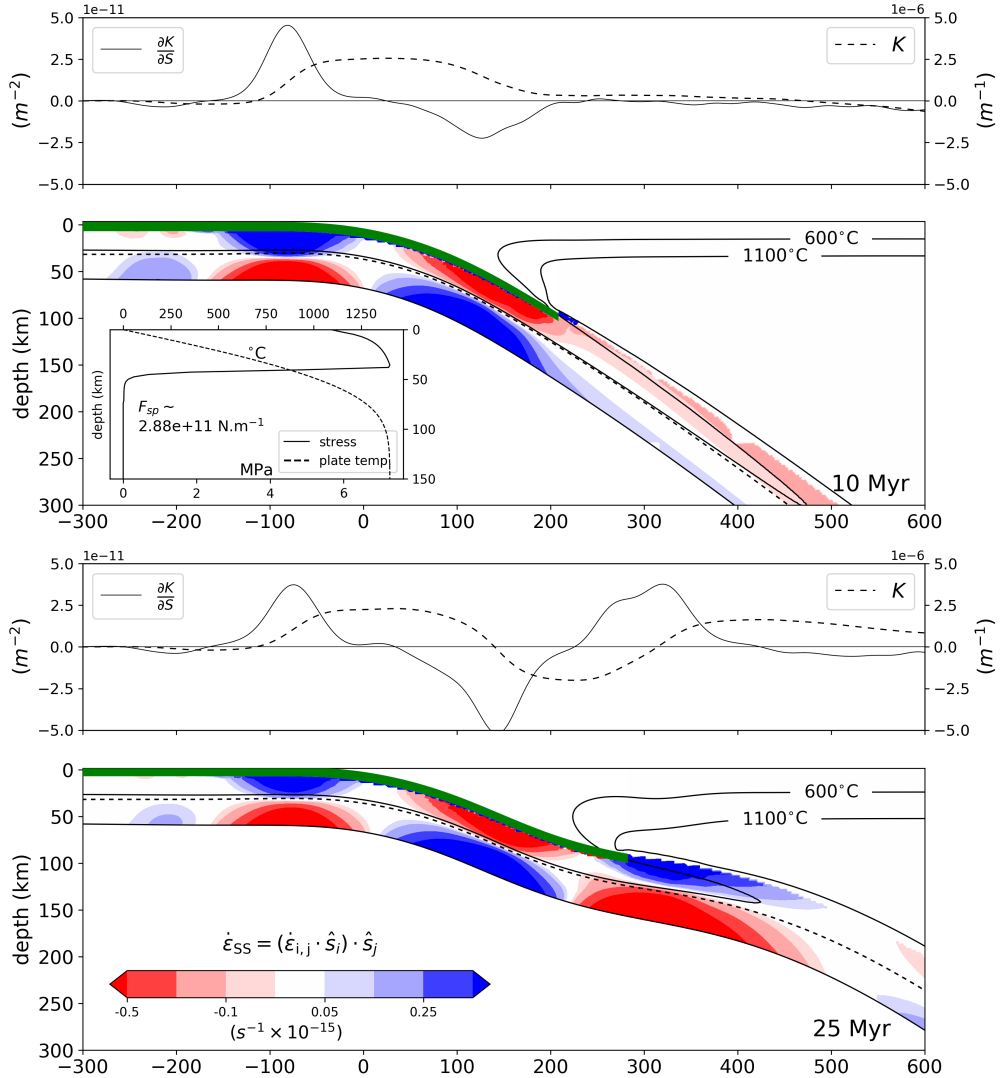


Figure 16. Strain rate distribution in numerical model at 10 Myr and 25 Myr. In each figure. The main panels show the downdip strain rate component in the slab ($\dot{\epsilon}_{ss}$) resolved parallel to the slab midplane. We show only the strong interior part of the slab: the subduction interface zone, upper plate, and parts of the mantle are above 1100°C isotherm have been masked. +ve values (blue) show zones of downdip extension, -ve values (red) are shortening. Solid black lines show isotherms as labelled. Dashed black line is the slab midplane. Shaded green region represents the subduction interface. Inset in the panel at time 10 Myr shows the temperature and stress (horizontal component) profile in the plate at 300 km to the LHS of the trench. The smaller upper panels shows the curvature and curvature gradient of slab midplane, plotted along the same horizontal axes as the main panels (distance from trench).

640 lier figures, the T-axes are projections on to a trench normal plane, but here they are
 641 rotated so that the angle relative to the midplane is preserved.

642 Figs. 17-19 show seismicity geometry relationships for the wPac regions. In the up-
 643 per panel, we show the rotated T-axes. In the lower panels we show histograms repre-
 644 senting the number of intra-slab earthquakes per unit distance along the midplane (note
 645 this is not equivalent to the total strain or moment release). Curvature and curvature
 646 gradient are plotted on the same horizontal axis (representing distance along the mid-
 647 plane) as indicated in figure legends. The curvature gradient profiles associated with wPac
 648 slabs reflect the relatively simple morphology of the slab hinge. In the plate bending re-
 649 gion, curvature gradients show a relatively symmetric positive peak, with a half-wavelength
 650 of between 150 - 200 km. Peak curvature (zero gradient) occurs at a considerable dis-
 651 tance (50 - 100 km) downdip from the trench. Beyond this, the downdip gradient changes
 652 sign and thereafter tends to decay monotonically as the slab straighten out in the mid
 653 upper mantle. In the wPac, OBZ earthquakes tend to center either near the peak in pos-
 654 itive curvature gradient (e.g. Kuriles), or in between the peak in curvature gradient and
 655 the peak in curvature (e.g. Japan, Tonga), but not at the peak in curvature.

656 The point where the curvature gradient switches sign is generally coincident with
 657 the transition between the OBZ earthquakes (DT earthquakes above the midplane), and
 658 the DSZs that we interpret (following many others) as being related to unbending (i.e.
 659 the PUZ, with DC earthquakes above the midplane, DT beneath). This transition does
 660 not necessarily represent a sharp inversion in the orientation of T-axis. In the Kuriles,
 661 for instance, a zone of several tens of kms exists where T-axes are somewhat random,
 662 before the unbending DSZ emerges. In Japan, the transition to negative curvature gra-
 663 dient coincides with the onset of upper-plane DC seismicity, but the onset of lower plane
 664 DT events does not appear to commence until about 100 km downdip of the transition.
 665 Clearly there are complexities in the relative number of upper plan (DC) and lower plane
 666 (DT) events, as evidenced by the strong asymmetry we see in the Tonga DSZ, versus much
 667 more symmetrical distribution in the Kuriles. Nevertheless, the orientation of seismic-
 668 ity in wPac slabs - particularly the upper plane seismicity - varies in a systematic way
 669 with the slab curvature gradient.

670 Corresponding seismicity geometry relationships for the ePac slabs are shown in
 671 Figs. 20, 21, and 22. As we noted in Section 4, there are far fewer OBZ earthquakes in

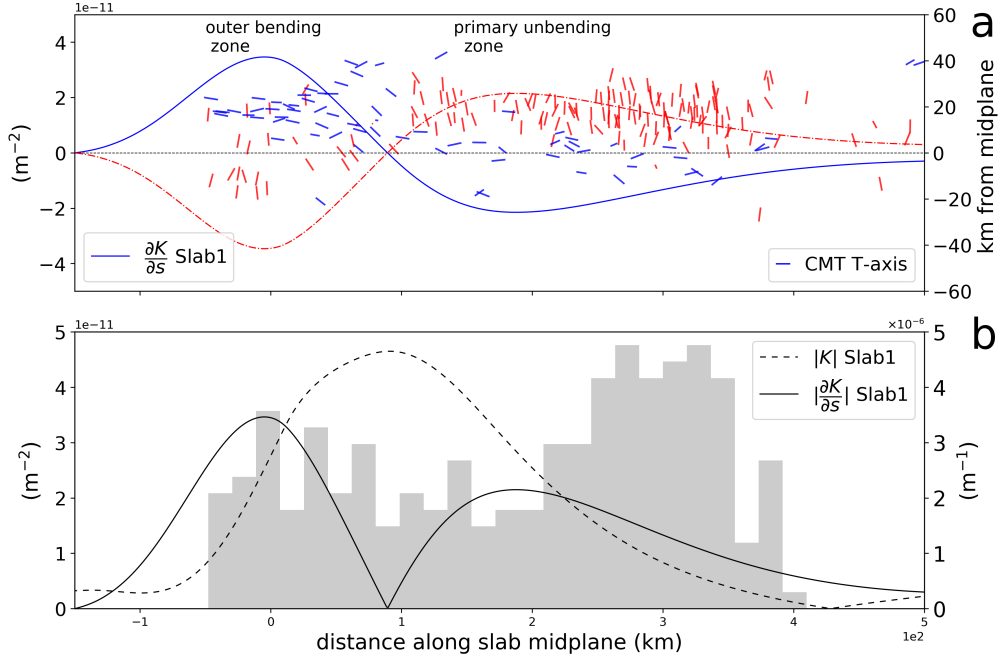


Figure 17. Summary of Tonga slab seismicity-geometry relationships. a) CMT T-axes are plotted in a slab midplane coordinate system, with distance from the hypocenter to the midplane shown on the vertical axis, and distance along the midplane relative to the trench (horizontal axes). The T-axes have been rotated so that the angle relative to the midplane is preserved. As in Fig. 6, the T-axes of the CMT moment tensors are plotted as uniform-length vectors, projected along a trench-perpendicular vertical plane. The length variation in the plotted T-axes reflects the magnitude of the projected component of the vector. The blue solid line shows the value of the curvature gradient plotted against the distance along the midplane. The red dashed line shows the reflection of the curvature gradient about the midplane. Together, these lines show parts of the slab that are expected to be stretching (blue half) and shortening (red half), due to the advective component of the bending rate; b) Histogram shows the relative variation in number of slab earthquakes as a function of distance along the midplane (earthquakes deeper than 300 km are excluded). Solid and dashed lines show the absolute value of the midplane curvature and the curvature gradient.

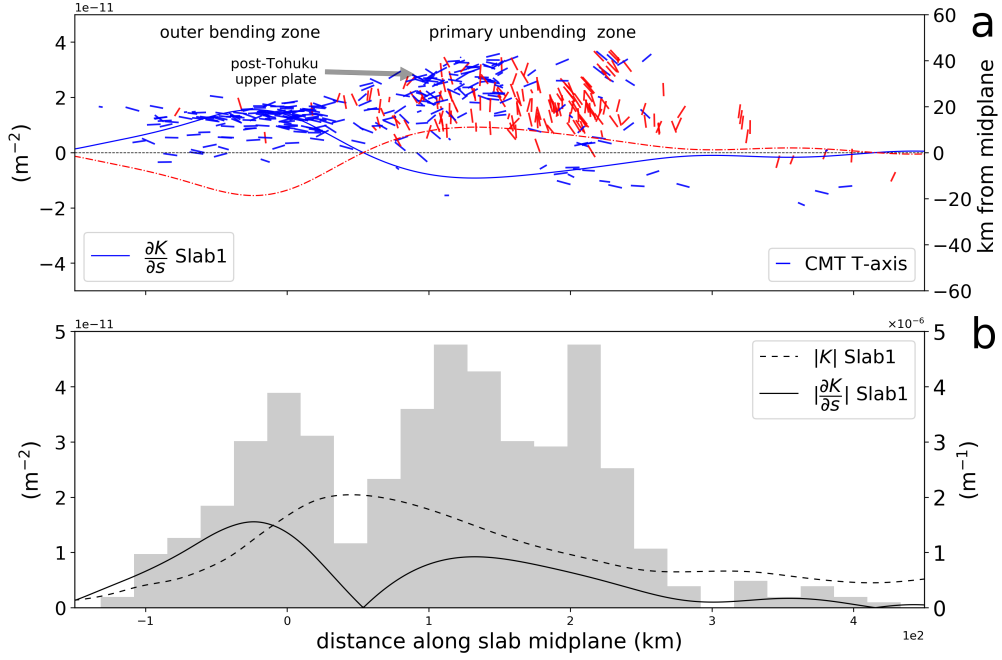


Figure 18. Summary of Japan slab seismicity-geometry relationships. See Fig. 17 caption for details of figure organisation and presentation.

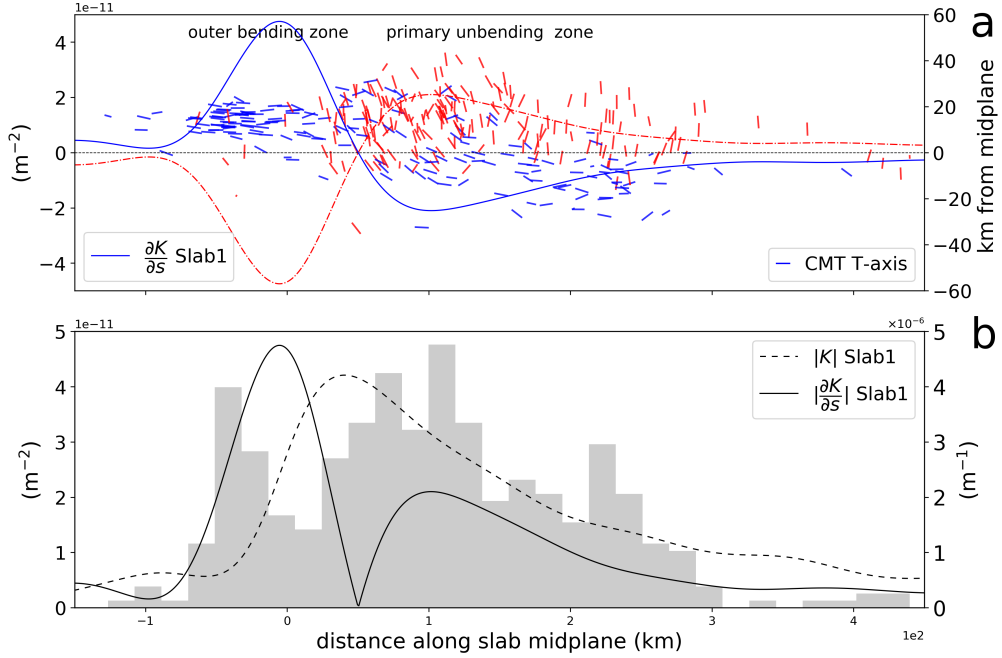


Figure 19. Summary of Kuriles slab seismicity-geometry relationships. See Fig. 17 caption for details of figure organisation and presentation.

672 the ePac regions. The small number that do occur, cluster on the landward side from
 673 positive peak in curvature gradient. In Peru these plate bending events occur virtually
 674 underneath the trench. Again we note that these do not coincide with peak curvature,
 675 but tend to cluster between the peak in curvature gradient and the peak in curvature.

676 In Chile and Peru, the point where the curvature gradient switches sign is also co-
 677 incident with the transition between the OBZ cluster (DT earthquake above the mid-
 678 plane), and the PUZ (DC earthquakes above the midplane). Figs. 20 and Fig. 21 shows
 679 that the PUZ events are clustered where the curvature gradient predicts maximum rates
 680 of unbending. Hence, while unbending earthquakes in the ePac slabs occur at shallower
 681 depths than the wPac, the distributions are consistent with same basic mechanism. There
 682 is no clear evidence of unbending-related earthquakes in central America. Moreover the
 683 zone of normal faulting, associated with plate bending, seems to continue in the land-
 684 ward direction, past the point when the curvature gradient changes sign. These patterns
 685 are difficult to interpret, and clearly do not fit with the systematic variation between plate
 686 bending - slab unbending, that we see in the other regions.

687 Whereas the wPac slabs unbend monotonically, the ePac slabs all exhibit additional
 688 zones of positive (and negative) curvature gradients. In Chile, a zone of positive curva-
 689 ture gradient begins at about 200 km downdip from the trench (Fig. 20) corresponding
 690 to the zone where the partially flattened slab begins to increase in curvature, and there-
 691 after dip more steeply toward the transition zone. Because of the curvature increase, the
 692 upper half of the slab is predicted to be undergoing extension. This zone has a strong
 693 spatial overlap with the belt of DT seismicity along the Chile slab at ~ 100 km depth,
 694 the most active part being the north Chile seismic belt (see Fig. 9). The full downdip
 695 seismic expression Chile, shows a remarkable set of transitions, where earthquakes in the
 696 upper half of the slab change from DT (OBZ) to DC (PUZ) and then back to DT where
 697 the slab is partially flattened, each transition correlating with the changing sign of the
 698 curvature gradient. Low seismic activity prevails in the intervening regions where bend-
 699 ing rates are predicted to be negligible. This is very much analogous to the deformation
 700 pattern exhibited in the numerical model.

701 Two potential inconsistencies arise in trying to connect the intermediate depth earth-
 702 quake belt in Chile with bending. The first is that in the CMT catalog, there is no in-
 703 dication of a lower plane of DC seismicity (although Comte et al. (1999) showed they

may be present in micro-seismicity). Nevertheless, as we summarise in the Discussion, such asymmetry seems to be the normal expression in zones where slab curvatures is increasing. The second problem is that, as we see in Fig. 12 and Fig. 20, a smaller number of DT events seem to lie well below the inferred midplane, a pattern that would seem to be more consistent with uniaxial stretching of the slab. We need to recall, however, that some variability in the lateral morphology of the slab occurs, due to the significant distance across which we aggregate the seismicity (as discussed in Section 2). Moreover, this variability tends to increases with depth (or at least distance from the trench). In Fig. B.2 we show a cross section for a much narrower lateral extent within the north Chile seismic belt (see figure caption for details). In this smaller region, the hypocenter locations are predominately located in the upper $\sim 10\text{-}20$ km of the slab, consistent with seismicity being localised above the neutral plane. However, we note that some deeper events - potentially outliers - still remain.

In Peru, earthquakes in the PUZ transition to sparse DT seismicity in the flat slab. The intensity of this DT seismicity increases towards the distal hinge of the flat slab. Fig 21 shows that curvature gradients are generally positive, although small, within the Peru flat slab. They increase rapidly towards the distal hinge of the flat slab, consistent with the increase in seismicity. As in Chile, the bending associated with these positive curvature gradients will create extension above the slab midplane. Hence, it plausible that the DT seismicity is the expression of upper plane events in a bending slab. If DT earthquakes in Peru are related the upper-plane of bending zones, it means that, like Chile, shortening below the neutral plane must be entirely aseismic. The idea that these DT earthquakes are upper-plane conflicts with the impression that, many of the Peru flat slab DT events appear to be beneath the inferred midplane (based on the region averaged Slab2 model). Again, we think it is plausible that is artifact due to unconstrained variations in the slab morphology.

In Fig. 21 we see a group of slightly deeper earthquakes cluster at the far landward edge of the domain (> 650 km along the slab midplane), located beyond the zone of positive curvature gradient. These have been highlighted using a greater transparency level, and are excluded from the histogram in the lower panel of Fig. 21. These are mainly events in the Pucallpa seismic nest (see Fig. 10 upper panel). It is reasonable to assume these are associated with a localised geometric discontinuity in the slab, which is unrelated to the advective bending signal we are trying to resolve (Gutscher et al., 2000; Wagner &

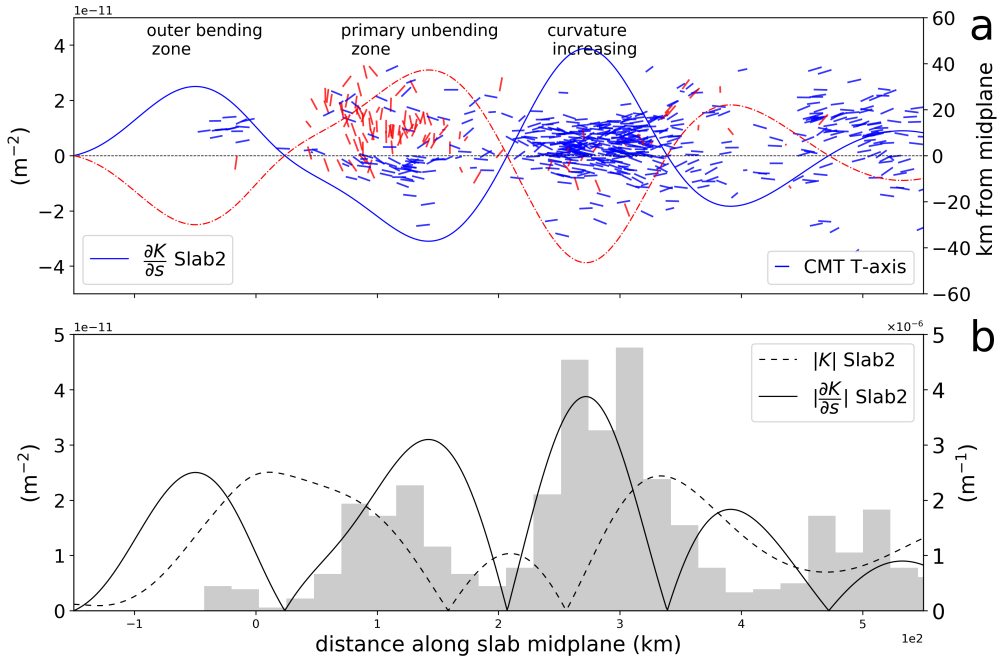


Figure 20. Summary of Chilean slab seismicity-geometry relationships. See Fig. 17 caption for details of figure organisation and presentation.

Okal, 2019). Recall that the advective bending signal we explore, inferred through curvature gradient, contains no information about lateral geometric variations, or time-dependent modes of deformation (i.e. changes in slab geometry that are occurring in an upper plate reference frame).

7 Discussion

7.1 Ubiquity of bending/unbending

In reference to northern Japan, Kawakatsu (1986a) argued that peak rates of geometric unbending (i.e. the advective bending rate) were likely to be higher than uniform stretching due to slab pull. Yet it is only in a few regions, northern Japan, Kuriles and Aleutians, where unbending has been recognised as a dominant control on slab seismicity. In particular, the role of unbending has very seldom been discussed in the context of ePac slabs (Isacks and Barazangi (1977) is one study we are aware of). In this study we have shown that earthquakes consistent with unbending are present in both wPac and ePac margin slabs. The region of Central America considered here is an exception, with no clear DC earthquakes. We note, however, that along other sections of the Mid-

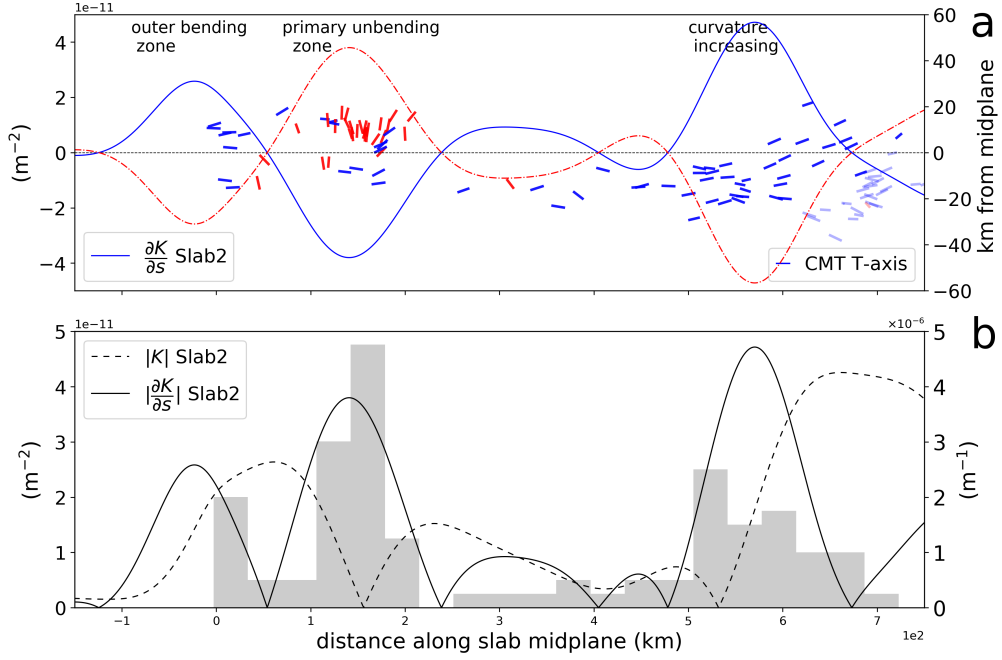


Figure 21. Summary of Peruvian slab seismicity-geometry relationships. See Fig. 17 caption for details of figure organisation and presentation.

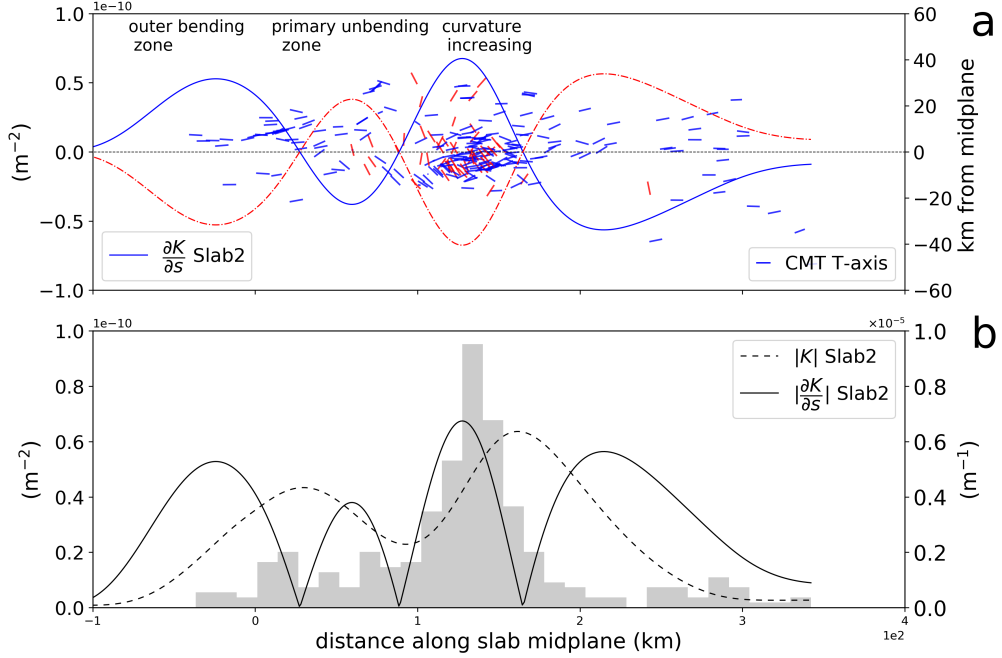


Figure 22. Summary of Central American slab seismicity-geometry relationships. See Fig. 17 caption for details of figure organisation and presentation.

752 dle America Trench, DC earthquakes characteristic of unbending are present (i.e. in the
 753 Mexican Flat slab region, see D. Sandiford, Moresi, Sandiford, and Yang (2019)). In most
 754 cases the PUZ is expressed as a polarised DSZ, with DC earthquakes occurring above
 755 (in a slab normal sense) a deeper band dominated by DT mechanisms. These polarised
 756 DSZs are consistent with the seismic expression of stretching/shortening either side of
 757 the neutral plane. However, the relative number of DT earthquakes compared to DC is
 758 quite variable, as exemplified in the difference between Tonga and Kuriles (c.f. Fig. 6
 759 and 8). We discuss this variability in the following sections.

760 The depth where PUZ earthquakes cluster varies substantially, with the ePac zones
 761 being consistently shallower depths than wPac. These variations are consistent with sys-
 762 tematic variations in slab geometry, whereby ePac slabs unbend at correspondingly shal-
 763 lower depths. The fact that ePac PUZs are shallower than the normal intermediate depth
 764 specification (> 70 km), may be one reason they have been somewhat neglected. In any
 765 case, the close proximity of ePac PUZ events to the megathrust means that filtering the
 766 signal from the latter is critical. Resolving the ePac PUZ requires aggregated along large
 767 lateral distances, at least when considering events within the magnitude range of the CMT
 768 catalog.

769 The occurrence of isolated DC earthquakes in the unbending zone of the Chile slab
 770 was noted by Lemoine et al. (2002), who proposed the term ‘slab push earthquakes’ to
 771 describe them, so as to distinguish them from more typical ‘slab pull’ (i.e. DT) earth-
 772 quakes. While Lemoine et al. (2002) mention a possible relationship between the DC events
 773 and slab unbending, they do not interpret the entire set of shallow intraslab earthquakes
 774 (both DC and DT) as a DSZ associated with unbending. Isacks and Barazangi (1977)
 775 suggest that DC earthquakes in Peru are related to unbending, an interpretation that
 776 our study supports. Fuenzalida, Schurr, Lancieri, Sobiesiak, and Madariaga (2013) pro-
 777 vide high-resolution aftershock solutions following a medium size DC event in the un-
 778 bending zone of the Chile slab (Mw 6.1 Michilla Earthquake, Dec. 16, 2007). The af-
 779 tershock sequence delineates a near-vertical fault plane between about 40 and 50 km depth.
 780 This orientation is consistent with reactivation of a steep landward-dipping outer-rise
 781 normal fault plane, and provides an important insight into the rupture character of a shal-
 782 low DC unbending event. The identification of a compelling unbending signal in the Nazca
 783 plate in Chile and Peru is important in the context of thinking about the overall dynamic
 784 state of the slab. Following (Kawakatsu, 1986a) it means that in the PUZ, rates of short-

785 ening above the neutral plane must exceed the ‘background’ rate of uniform stretching.
 786 This does not rule out, of course, that stretching rates may be non-uniform, and could
 787 for instance become larger at depths beyond the PUZ (e.g. Bloch et al., 2018). Overall,
 788 our results strongly support Kawakatsu’s argument about the relative magnitudes of ge-
 789 ometric unbending versus uniform stretching.

790 7.2 Geometric bending and contrasting seismic expression

791 The role of geometric bending has mainly been explored in relation to wPac slabs,
 792 where the process of unbending (PUZ) occurs over a larger downdip distance and peaks
 793 at greater depth than ePac. In the wPac slab regions we have considered, inferred rates
 794 of unbending decay monotonically as slabs straighten out in the mid-upper mantle, con-
 795 sistent with the gradual falloff in seismicity. These wPac-type slab morphologies are of-
 796 ten presented as the archetypal subduction geometry. However, subduction along much
 797 of the ePac margin is characterised by alternating fully and partially flattened slab sec-
 798 tions. While constraining the precise geometry of ePac slabs remains a challenge, the gen-
 799 eral picture of these more complex morphologies is fairly well established (Engdahl et
 800 al., 1998; Hayes et al., 2018; Isacks & Barazangi, 1977). We argue that these systematic
 801 geometric differences are the key control on the contrasting seismic expression of ePac
 802 and wPac slabs at intermediate depths. Analysis of the downdip curvature gradient shows
 803 that the Nazca plate fully unbends at depths of around 60 km. Beyond this, additional
 804 zones of bending occur, which are associated with full or partial slab flattening. The ma-
 805 jority of ePac DT seismicity is conspicuously clustered in curvature-increasing zones. We
 806 summarise these systematic geometric differences between wPac and ePac in Fig. 23.

807 If advective bending is the dominant control for localising DT seismicity in ePac
 808 slabs, it requires that the lower half of the bending regions (i.e. beneath the neutral plane)
 809 is almost completely aseismic. In this light an important observation is that an oppo-
 810 sitely polarised DSZ has been observed in microseismicity, near the northern limit of our
 811 Chile study region (18°S) (Comte & Suarez, 1994).

812 Micro-seismicity aside, the lack of significant lower plane events in these putative
 813 bending zones, like the north Chile seismic belt, may seem at odds with the presence of
 814 lower plane events updip in the PUZ. However, this actually follows a pattern that is quite
 815 consistent, throughout different depths, in most subduction settings we analyse. Specif-

816 ically, it appears that the seismic expression of zones of increasing curvature tends to more
 817 asymmetric (less lower plane activity) than the expression of decreasing curvature. For
 818 instance, the OBZ is normally dominated by upper plane DT events, whereas in the PUZ,
 819 we tend to see lower plane events more strongly. A simple explanation for this is that
 820 the flexural stress state is modified by a uniaxial component, due to slab pull, acting in
 821 a sense of effective tension. This is expected to modify the relative depth of the neutral
 822 plane of bending (e.g. Craig et al., 2014). In zones of increasing curvature, the flexural
 823 stress state in the upper half of the slab is tensional (see next Section for discussion of
 824 relationship between stress and strain rates). Relative to pure bending, a uniaxial ten-
 825 sional component would be expected to shift the neutral plane deeper, closer to, or even
 826 beyond the brittle ductile transition, at around 600 - 700 °C. In zones of decreasing cur-
 827 vature, the opposite applies, with the neutral plane shifting towards the slab surface into
 828 colder parts of the slab, enhancing the prospect of seismic strain occurring beneath the
 829 neutral plane. This describes a systematic pattern we see in the Kuriles, Japan, Chile
 830 and Peru. Hence, the absence of lower plane events in the north Chile seismic belt, or
 831 the Peru flat slab, is compatible with a similar absence in the OBZ of the Kuriles and
 832 Japan.

833 In this context Tonga is anomalous in that the pattern is systematically reversed
 834 compared to the other slabs. In Tonga, we observe a more symmetric pattern, charac-
 835 terised by numerous lower plane earthquakes in the OBZ, and a less symmetric pattern
 836 with far fewer lower plane earthquakes in the PUZ. This could indicate that, relative to
 837 other settings, the magnitude of the uniaxial stress component due to slab pull is reduced
 838 (or possibly even reversed). This concurs with earlier ideas that the seismic expression
 839 in Tonga has a more compressive signal than other slab regions (Gurnis et al., 2000; Isacks
 840 & Molnar, 1971; Nothard, McKenzie, Haines, & Jackson, 1996). Alternatively, a signif-
 841 icant change in slab strength profile may also alter the depth of the neutral plane (e.g
 842 Craig et al., 2014). However, the systematic reversal of the DSZ symmetry patterns, with
 843 respect to the other slabs, is most easily explained through the effect of a uniaxial stress
 844 component.

845 7.3 Slab rheology, strain rates and elasticity

846 It is well understood that deformation of the lithosphere is accommodated by elas-
 847 tic as well as a range of inelastic mechanisms. Investigations focused on the loading of

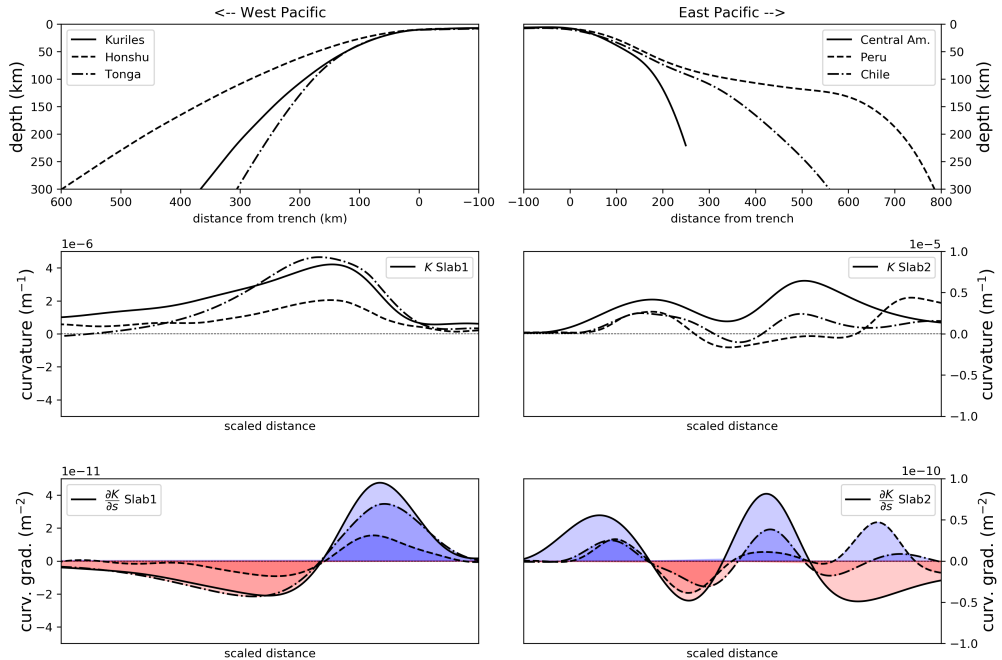


Figure 23. Comparison of characteristic features of wPac (left) and ePac (right) slab geometries. Upper panel shows slab profiles, middle panel shows curvatures and lower panels show curvature gradients. The advective rate of bending is governed by the curvature gradient. In the lower two panels (either side) we have scaled the horizontal distance (distance along the mid-plane) so that the transition from the OBZ to the PUZ lies at the same point (i.e. the first zero crossing of the curvature gradient is equal for the ePac and wPac groups respectively).

848 oceanic lithosphere, including the bathymetry profile of plates near the trench, has tended
 849 to emphasise the elastic nature of plates. On the other hand, the existence of earthquakes,
 850 along with a range of other inferences, suggests that inelastic deformation must account
 851 for much of the total strain accumulation during bending in the subduction hinge (Billen,
 852 2005; Chapple & Forsyth, 1979; Engdahl & Scholz, 1977; Sleep, 1979).

853 Turcotte, McAdoo, and Caldwell (1978) argued that the Kuriles bathymetry was
 854 consistent with the bending of a constant thickness elastic plate, while the more strongly
 855 curved Tonga profile implied a significant region of plastic failure in the plate. McAdoo,
 856 Caldwell, and Turcotte (1978) argued that the Kuriles bathymetry was better fit by an
 857 elasto-plastic rheology. These conflicting findings reflect differing assumptions, such as
 858 the magnitude of the in-plane compressive force, which is finite in the McAddoo model,
 859 as well as the initial elastic thickness of the undeformed lithosphere. Recent global anal-
 860 yses have argued that weakening of the plate, with an associated reduction in the elas-
 861 tic thickness at the outer rise, uniformly improves the fit of predicted profiles to observed
 862 bathymetry and gravity (Hunter & Watts, 2016). Hence, while early studies seemed to
 863 show that plates, at least in some cases, exhibited a purely-elastic response in the vicin-
 864 ity of the trench, ongoing work casts doubt on this result.

865 At peak curvature the potential elastic stress in slabs is of the order of 10 GPa (e.g.
 866 D. Sandiford et al., 2019). Because this is at least an order of magnitude larger than in-
 867 ferred slab yield stresses (Chapple & Forsyth, 1979), inelastic yielding would be expected
 868 to accommodate the large proportion of bending strains in slabs (Engdahl & Scholz, 1977;
 869 Wang, 2002). As previous studies have noted, a primary mechanism for plastic strain
 870 at yield is the slip accompanying earthquakes (Chapple & Forsyth, 1979; Sleep, 2012).
 871 An important consequence of inelastic deformation is the fact that the flexural stress state
 872 is often inverted with respect to the sign of the slab curvature. Indeed the premise that
 873 earthquakes occur as a response to slab unbending (where the curvature is still positive)
 874 reflects the assumption of significant inelastic deformation. We argue that in the limit
 875 of very weak slabs, where the majority of strain is accommodated by inelastic deforma-
 876 tion, the flexural stress state will tend to approximate the bending rate, not the curva-
 877 ture. When the sign of the bending rate changes, the flexural stress will rapidly (com-
 878 pared to the change in the sign of the curvature) evolve to match the sign (polarity) of
 879 the bending rate. In this study we have emphasised that, to first order, the orientation
 880 of seismic moment tensors correlates with the inferred bending rate (i.e. curvature gra-

881 dient), rather than total strain (i.e. curvature). This relationship supports previous work
 882 suggesting that slabs must yield rapidly after the onset of bending in the hinge (Billen,
 883 2005; Engdahl & Scholz, 1977; Sleep, 2012).

884 7.4 Implications for subduction dynamics

885 The sources of buoyancy that drive plate motions are often separated into density
 886 anomalies in the surface plates (e.g. ridges and other topography) and sublithospheric
 887 sources (e.g. slabs) (e.g Coblenz, Richardson, & Sandiford, 1994; Ghosh, Holt, & Flesch,
 888 2009). How much of the slab density deficit is propagated through the slab into the sur-
 889 face plates has been an ongoing debate in geodynamics. Attempts to understand the global
 890 distribution of plate velocities, for instance, have concluded that a large fraction of slab
 891 weight must be propagated through the slab (Conrad & Lithgow-Bertelloni, 2002; Forsyth
 892 & Uyeda, 1975; van Summeren, Conrad, & Lithgow-Bertelloni, 2012). While the pres-
 893 ence of intermediate depth DT zones does not constrain the magnitude of stress in slabs,
 894 the inference of uniform stretching in slabs is clearly compatible with the idea that stresses
 895 due to slab pull are significant (e.g. Molnar & Bendick, 2019). With simple assumptions
 896 made about effective slab rheology, stresses in the order of 100s of MPa, have previously
 897 been estimated (Conrad & Lithgow-Bertelloni, 2004). While the notion that slabs un-
 898 dergo uniform stretching seems consistent with inferences about the forces driving plate
 899 motion, the paradox remains as to why the seismic expression of ‘slab pull’ is evidently
 900 not expressed in wPac slabs, which are attached to the fastest moving large plate. One
 901 suggestion is that these DC slabs subduct at rates faster than their terminal (Stokes)
 902 sinking velocity, and hence undergo uniform shortening (Forsyth & Uyeda, 1975; Fujita
 903 & Kanamori, 1981b).

904 Other lines of evidence suggest slab pull must be significantly smaller than inferred
 905 from plate velocity considerations. Coblenz et al. (1994) argued that the intraplate stress
 906 field is largely explicable in terms of a balance between lithospheric potential-energy dis-
 907 tribution and plate-boundary resistance, implying a relatively low degree of slab-plate
 908 coupling in plates is the norm. These results are implicit in other modelling studies, which
 909 capture the first order features of the intraplate stress field without considering any sub-
 910 lithospheric sources (e.g. Ghosh et al. (2009)). Based on stress indicators in the central
 911 Indian Ocean M. Sandiford, Coblenz, and Schellart (2005) showed that the effective slab
 912 pull fraction must be low, around 0.1 in order to account for large magnitude reverse fault

913 mechanisms observed in the central Indian Ocean with P-axes parallel to the Sumatran
 914 trench, implying a average deviatoric tensional stress no more than order 10 MPa prop-
 915 agated via the slab.

916 The dominant control of bending over stretching in slab seismic strain release is
 917 a characteristic of slabs in the Stokes regime, where resistance to slab weight is primar-
 918 ily supplied by drag from the mantle (F. A. Capitanio et al., 2009; Goes, Capitanio, Morra,
 919 Seton, & Giardini, 2011). In this study we highlight that slabs in the Stokes regime can
 920 develop highly-diverse internal deformation patterns. The diversity in strain patterns
 921 in slabs arises from the curvature-gradient dependence of the advective bending rate. We
 922 show that the pervasive DT expression of slab in the ePac appears to be linked to zones
 923 of curvature increase at intermediate depths. Relatively subtle changes in slab morphol-
 924 ogy, such as the partial flattening of the slab in northern Chile, create alternating zones
 925 of bending and unbending over relatively short wavelengths. A feature of our framework
 926 is that it obviates special appeals to fundamental differences in slab stress (or strength)
 927 between different slabs, such as is required in the conventional interpretation of uniform
 928 stretching in Chile, and shortening in Tonga (e.g. Fujita & Kanamori, 1981b; Isacks &
 929 Molnar, 1971).

930 In the framework we propose, contrasts in ePac and wPac seismic expression arise
 931 due to systematic differences in slab morphology. In the ePac, zones of positive bend-
 932 ing rate are associated with full or partial slab flattening. Recent work suggest that these
 933 slab-morphology contrasts may be controlled by kinematics of the upper plates with re-
 934 spect to large-scale mantle flow (Yang et al., 2019). Atlantic Ocean opening allows fast
 935 trench-ward motion of South America, which promotes compression-dominated tecton-
 936 ics in the overriding plate, that has been argued to provide the pre-conditions for flat-
 937 slab development along the ePac margin (Manea & Gurnis, 2007; W. Schellart, 2017; van
 938 Hunen, van den Berg, & Vlaar, 2004; Yang et al., 2019). In contrast, large-scale down-
 939 welling beneath Asia, revealed by seismic imaging, geodynamic models, and plate recon-
 940 structions seems to restrain trench-ward motion of East Asia. Along with the greater
 941 ages of wPac slabs, this promotes steeper subduction, and extension-dominated upper-
 942 plate tectonics (Yang et al., 2019).

943 Our framework also provides an interesting perspective on the dynamics of intra-
 944 continental intermediate depth seismic zones such as Hindu Kush and the Vrancea zone

beneath the Carpathians, where seismic strain rates exceed $10^{-14} s^{-1}$ (Lorinczi & Houseman, 2009; Molnar & Bendick, 2019). These are an order of magnitude greater than typical intermediate depth seismic strain in subducting slabs ($\sim 10^{-15} s^{-1}$). The strain rates beneath the Hindu Kush and Vrancea are consistent with a regime of uniform stretching associated with lithospheric necking (Lister, Kennett, Richards, & Forster, 2008; Lorinczi & Houseman, 2009). It is precisely because DT slabs (e.g. Chile) are not necking that seismic strain rates are much lower. They are, instead, controlled by rates of geometric bending, which reconciles the observed seismic release rates closer to $10^{-15} s^{-1}$) (Kawakatsu, 1986a).

954 7.5 Limitations and future work

In trying to establish the basic spatial correlation between bending rates and slab seismicity, we have focused on the advective component of the bending rate (Buffett, 2006; Ribe, 2001, 2010). The time-independence allows us to infer the relative variation in long-term bending rates from present day slab geometry. The advective component of the bending rate should be the dominant bending term for slabs in which: a) the hinge morphology is not changing rapidly, and b) three-dimensional (along-strike) contributions to the stress/deformation are relatively minor (Buffett & Becker, 2012; Buffett & Heuret, 2011). Clearly these conditions may not be met in all slab regions, and this caveat will require careful attention in trying to test this hypothesis in other settings. In this study we have primarily focused on the variation in the orientation of seismicity (moment tensors) with respect to slab geometry (curvature gradient). We have been more circumspect about the correlation between seismicity rates and the relative magnitude of the curvature gradient. This is primarily because seismic activity rates are not necessarily proportional to the long term strain rate (i.e. the bending rates inferred via the curvature gradient). The influence of metamorphism and fluids is one effect which is likely to effect the rates of seismicity. It was shown, for instance, that the intermediate depth seismic activity rate varies with the inferred amount of plate hydration in the outer-rise region (Boneh et al., 2019), with similar mechanisms being linked to rapid changes seismic expression along-strike (Shillington et al., 2015). This process is a potential control on dramatic changes in seismic activity rates between the north Chile seismic belt, and parts of the Nazca slab further south (e.g. Fig. 9). Another factor to consider is simply the increasing role of ductile deformation as the slab heats up from above and below. As a result, the relative

amount of seismic/ductile deformation is likely to vary in a complex manner with changes in pressure and temperature. Finally, short catalog times are likely to also bias the relative number of earthquakes in different parts of the slab. We highlight, for instance, the increase in OBZ seismicity in Northern Japan following the Tohoku earthquake. The number of earthquakes is likely to include a range of transient signals.

In the regions we have addressed, there are number of instances where the correlation between curvature gradient and seismic expression is ambiguous, absent, or opposite to what we would expect. We briefly discuss a few of examples, some of which we think are readily explained, and some not. In the ePAc settings, we have discussed clusters of seismicity which are likely to be unrelated to the advective bending mode. The Pucallpa seismic nest in Chile is an example of a seismicity cluster that apparently correlates with a relatively localised trench-parallel perturbation of the slab morphology (Gutscher et al., 2000; Wagner & Okal, 2019). This is region where deformation of slab is likely to involve lateral, time-dependent changes in slab morphology.

In the case of Chile, we demonstrate a close spatial association between the main peak in positive curvature gradient (see Fig. 20) and the primary cluster of DT seismicity (the north Chile seimsic belt, see Fig. 9). However, the relationship becomes increasingly inconsistent at greater depths. Based on our geometric analysis, the slab would be expected to go through an additional zone of unbending (i.e. a secondary unbending zone), where the sign of the curvature gradient returns to negative (e.g. Fig. 20). This transition is also seen in the numerical model, which predicts a return to downdip shorting at around 550 km from the trench (which is seen in the far RHS in the lower panel of Fig. 16). And yet we see no persuasive evidence that DC earthquakes (e.g. upper plane unbending earthquakes) occur at this depth in Chile, or for that matter in Peru or Central America. These predicted secondary unbending zones are missing, and this remains difficult to explain in our framework, unless we appeal to increasing magnitude of slab stretching rates, relative to advective bending rates, at these depths (Bloch et al., 2018), or that the upper-part of slab has become by this stage aseismic (potentially through warming and/or dehydration).

1006 **8 Conclusions**

1007 Our study suggests that the ‘fingerprints’ of flexure in slab seismicity are more sig-
 1008 nificant than previously realised. We have analysed the contribution of the advective bend-
 1009 ing rate, and found that in several key locations, the orientation of slab seismic moment
 1010 tensors vary systematically with the anticipated sense of defomation. The fact that flex-
 1011 ure controls seismicity patterns in the plate bending domain (OBZ) is of course, already
 1012 widely accepted, as is the effect of unbending in a limited number of slab settings. In
 1013 terms of extending the role of bending/unbending, our contributions are twofold. Firstly
 1014 we show that seismicity characteristic of unbending is prevalent in ePac slabs, albeit at
 1015 shallower depths than wPac slabs. We then show that geometric differences between ePac
 1016 and wPac slabs lead to additional zones of bending at intermediate depths in ePac slabs.
 1017 The majority of ePac DT seismicity is conspicuously clustered in these curvature-increasing
 1018 zones, which are associated with full or partial slab flattening. Hence, the contrasting
 1019 seismic expression in ePac and wPac slabs appears to arise due to systematic differences
 1020 in slab morphology - rather than through significant differences in subduction force bal-
 1021 ance, as implied in previous conceptual frameworks. We argue that the observed corre-
 1022 lation of seismic of earthquake orientation with the curvature gradient (and not curva-
 1023 ture) arises from the fact that a very significant proportion of bending strain is accom-
 1024 modated by inelastic deformation, of which seismic slip itself is a key component.

1025 **A Numerical model setup**

1026 The model was developed using the Underworld2 code, and follows closely the setup
 1027 described in (D. Sandiford & Moresi, 2019), to which we refer readers for a description
 1028 of the governing equations, numerical method, mantle rheology, and implementation of
 1029 the subduction interface. Compared to (D. Sandiford & Moresi, 2019), we have made
 1030 two noteworthy changes in the setup of model discussed here: 1) We use a larger domain,
 1031 with a higher relative resolution; 2) we constrain the upper viscosity limit in a small part
 1032 of the mantle wedge to a value of 1. The geometry of the viscosity-limited section of the
 1033 wedge is shown in Fig. A.1. This element of the model constitutes a very simplified at-
 1034 tempt to account for processes such as the presence volatiles and melts in the wedge. These
 1035 are expected to substantially reduce the effective viscosity, compared to the dry melt-
 1036 free conditions that are reflected in our model creep law (diffusion creep). In terms of the
 1037 model evolution the viscosity limit applied to this region has the primary effect of allow-
 1038 ing asymmetric subduction to proceed even when the slab dip angle becomes quite shal-
 1039 low, and the upper plate has thickened (both due to cooling and a degree of shortening).
 1040 If we did not provide this upper limit on the viscosity, the shallow part of mantle wedge
 1041 would increase in viscosity as the slab dip decreases, due to reduction in temperature.
 1042 This creates increased coupling with upper plate, and a rapid feedback cycle that results
 1043 in a breakdown of single-sided subduction.

1044 Fig. A.1 provides an overview of the model domain, as well as initial and bound-
 1045 ary conditions. The depth of the domain is 1500 km, and the aspect ratio is 6. Initial
 1046 temperature conditions define two plates which meet at the centre of the domain, includ-
 1047 ing a small asymmetric slab following a circular arc to a depth of 150 km. The subduct-
 1048 ing plate has an initial age of 50 Myr at the trench, while the upper plate age is 10 Myr.
 1049 Both plates have a linear age profile with an initial age of zero at the sidewalls. This setup
 1050 allows the model to evolve under the driving force of internal density anomalies which
 1051 is therefore regarded as a fully dynamic model. Apart from the presence of a WL, there
 1052 is no compositional difference between the subducting and upper plate, nor do we in-
 1053 clude any compositional differentiation within the oceanic lithosphere. The only aspects
 1054 of the model setup that are varied are the details of subduction interface implemen-
 1055 tation (described in the following section) and the model resolution.

1056 Approximate solutions to the incompressible momentum and energy conservation
1057 equations are derived using the finite element code Underworld2. Underworld2 is a Python
1058 API which provides functionality for the modelling of geodynamic processes. Underworld2
1059 solves the discrete Stokes system through the standard mixed Galerkin finite element for-
1060 mulation. The domain is partitioned into quadrilateral elements, with linear elements
1061 for velocity and constant elements for pressure. Material properties are advected on La-
1062 grangian tracer particles.

1063 The model has a mesh resolution of 392 elements in the vertical direction, refined
1064 to provide an element width of ~ 1 km near the surface, and a particle density of 30 trac-
1065 ers per element. Particles are added and removed to maintain density near this value.
1066 During quadrature, material properties are mapped to quadrature points using nearest-
1067 neighbour interpolation. The Lagrangian tracer particles are used to distinguish the sub-
1068 duction interface material from the rest of the system (lithosphere and mantle). Under-
1069 world2 solves the energy conservation equation using an explicit Streamline Upwind Petrov
1070 Galerkin (SUPG) method. In this approach, a Petrov-Galerkin formulation is obtained
1071 by using a modified weighting function which affects upwinding-type behaviour. The Stokes
1072 system has free-slip conditions on all boundaries. The energy equation has constant (Dirich-
1073 let) and zero-flux (Neumann), on the top and bottom boundary respectively. The left
1074 and right sidewalls have a constant temperature equal to the mantle potential temper-
1075 ature (1673°K). The surface temperature is 273°K.

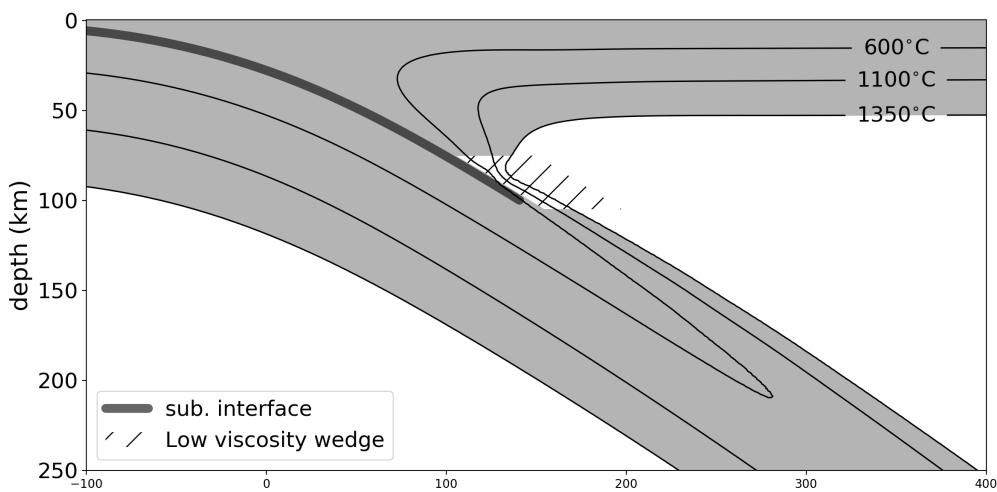


Figure A.1. Detail of numerical model at 10 Myr. The grey region shows parts of the model colder than 1350°C (model potential temperature is 1400 °C). The hatched region shows the part of the mantle wedge in which the upper limit of viscosity is set to 2×10^{20} Pa s.

Parameter name	Value	Symbol	Units
domain depth	1000	-	km
domain width	5000	-	km
potential temp	1673	T_p	K
surface temp	273	T_s	K
viscosity min.	1×10^{18}	-	Pas
viscosity max.	1×10^{24}	-	Pas
diffusion creep volume UM**	5.27×10^{-6}	V	$\text{m}^3 \text{ mol}^{-1}$
diffusion creep energy UM	316	E	kJ mol^{-1}
diffusion creep constant UM	1.87×10^9	A	$\text{Pa}^n \text{ s}^1$
diffusion creep volume LM***	1.58×10^{-6}	V	$\text{m}^3 \text{ mol}^{-1}$
diffusion creep energy LM	210	E	kJ mol^{-1}
diffusion creep constant LM	1.77×10^{14}	A	$\text{Pa}^n \text{ s}^1$
DP* friction coefficient	0.1	μ	-
DP cohesion	20	C	MPa
yield stress max.	200	τ_{\max}	MPa
sub. interface thickness	10	W_{init}	km
sub. interface max. thickness	19	W_{\max}	km
sub. interface min. thickness	10	W_{\min}	km
sub. interface viscosity	5×10^{19}	-	Pas
sub. interface depth taper start	100	-	km
sub. interface depth taper width	30	-	km
LVW† viscosity	2×10^{20}	-	Pas
LVW upper depth	45	-	km
LVW lower depth	150	-	km
slab age at trench	50	-	Myr
slab radius of curv.	200	-	km
initial slab depth	150	-	km
upper plate age at trench	10	-	Myr
lower mantle viscosity increase	15	-	-
adiabatic temp. gradient	3.7×10^{-4}	-	-
internal heating	0.0	Q	W.m^{-3}

Table A.1. Dimensional model parameters: * Drucker-Prager, ** Upper Mantle, *** Lower mantle. †: Low Viscosity Wedge. Typical model element resolution was 800×160 .

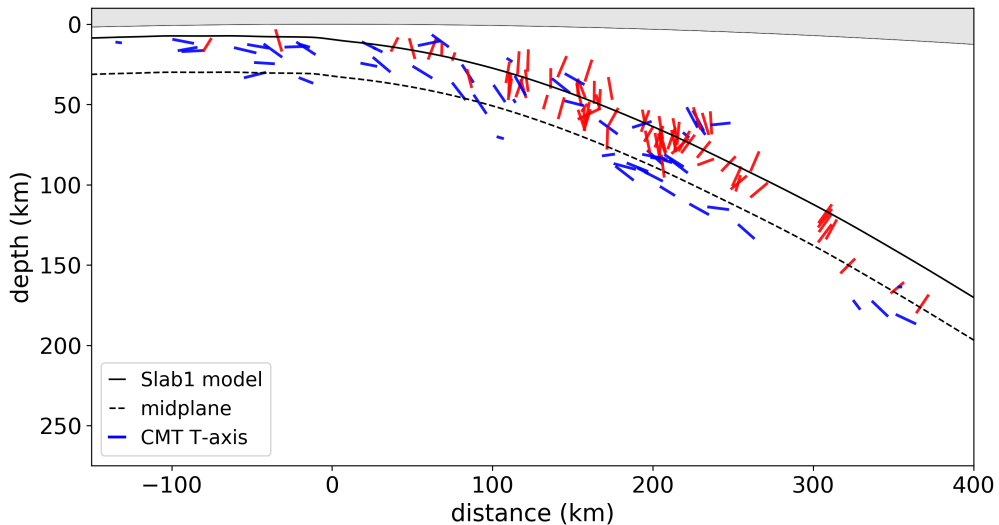


Figure B.1. Cross section of CMT T-Axes for Japan region (northern Honshu), for period before Tohoku earthquake (11/03/2011)

B Additional Figures

Acknowledgments

This work was supported by the Australian Research council (Discovery grant DP150102887). Development of the Underworld2 code (<http://www.underworldcode.org/>) was supported by AuScope. DS's postgraduate research at the University of Melbourne was supported by a Baragwanath Geology Research Scholarship. This work was supported by resources provided by The Pawsey Supercomputing Centre with funding from the Australian Government and the Government of Western Australia. This work was supported by the Nectar Research Cloud, a collaborative Australian research platform supported by the National Collaborative Research Infrastructure Strategy (NCRIS). The study benefited from discussions with Greg Houseman and Claire Currie.

References

- Amante, C., & Eakins, B. W. (2009). Etopo1 arc-minute global relief model: procedures, data sources and analysis.
- Bailey, I. W., Becker, T. W., & Ben-Zion, Y. (2009, June). Patterns of co-seismic strain computed from southern California focal mechanisms. *Geophysical Journal International*, 179(3), 1131–1146. doi:10.1046/j.1365-246X.2009.04272.x

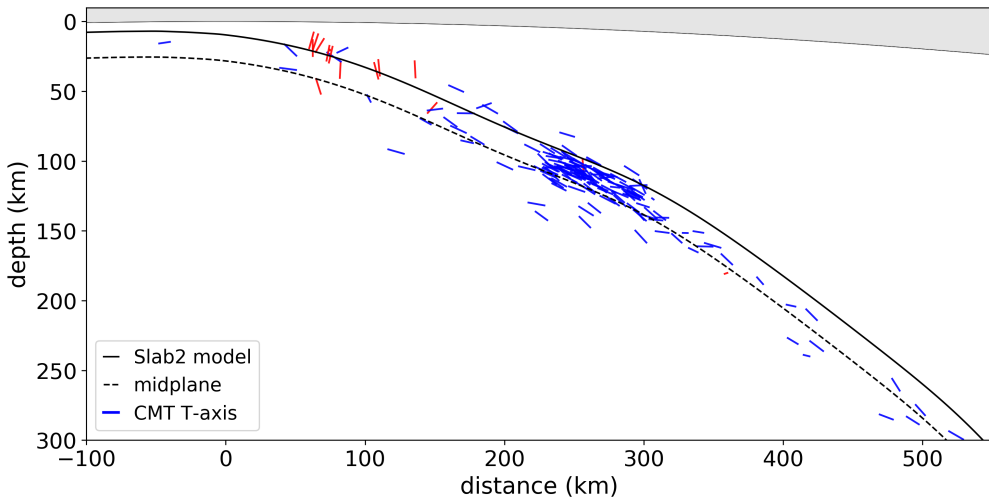


Figure B.2. Chile cross section for restricted domain, normal to the South American trench between 18.5° and 22° south. This region is also represented by the transparent green band in Fig. 9.

- 1092 *Journal International*, 177(3), 1015–1036. Retrieved from <https://doi.org/10.1111/j.1365-246x.2009.04090.x>
- 1093
- 1094 Barazangi, M., & Isacks, B. (1976). Spatial distribution of earthquakes and subduc-
1095 tion of the nazca plate beneath south america. *Geology*, 4(11), 686. Retrieved
1096 from [https://doi.org/10.1130/0091-7613\(1976\)4<686:sdoeas>2.0.co;2](https://doi.org/10.1130/0091-7613(1976)4<686:sdoeas>2.0.co;2)
1097 doi: 10.1130/0091-7613(1976)4<686:sdoeas>2.0.co;2
- 1098 Billen, M. I. (2005). Constraints on subducting plate strength within the Kermadec
1099 trench. *Journal of Geophysical Research*, 110(B5). Retrieved from <http://dx.doi.org/10.1029/2004jb003308> doi: 10.1029/2004jb003308
- 1100
- 1101 Billen, M. I., Gurnis, M., & Simons, M. (2003, May). Multiscale dynamics
1102 of the tonga-kermadec subduction zone. *Geophysical Journal Interna-*
1103 *tional*, 153(2), 359–388. Retrieved from <https://doi.org/10.1046/j.1365-246x.2003.01915.x> doi: 10.1046/j.1365-246x.2003.01915.x
- 1104
- 1105 Bloch, W., Schurr, B., Kummerow, J., Salazar, P., & Shapiro, S. A. (2018). From
1106 slab coupling to slab pull: Stress segmentation in the subducting nazca plate.
1107 *Geophysical Research Letters*, 45(11), 5407–5416.
- 1108
- 1109 Boneh, Y., Schottenhamel, E., Kwong, K., Zelst, I., Tong, X., Eimer, M., ... Zhan, Z. (2019, April). Intermediate-depth earthquakes controlled by incoming plate

- hydration along bending-related faults. *Geophysical Research Letters*, 46(7), 3688–3697. Retrieved from <https://doi.org/10.1029/2018gl081585> doi: 10.1029/2018gl081585
- Brudzinski, M. R., Thurber, C. H., Hacker, B. R., & Engdahl, E. R. (2007, jun). Global Prevalence of Double Benioff Zones. *Science*, 316(5830), 1472–1474. Retrieved from <http://dx.doi.org/10.1126/science.1139204> doi: 10.1126/science.1139204
- Buffett, B. A. (2006). Plate force due to bending at subduction zones. *Journal of Geophysical Research*, 111(B9). Retrieved from <https://doi.org/10.1029/2006jb004295> doi: 10.1029/2006jb004295
- Buffett, B. A., & Becker, T. W. (2012). Bending stress and dissipation in subducted lithosphere. *Journal of Geophysical Research*, 117(B5). Retrieved from <http://dx.doi.org/10.1029/2012jb009205> doi: 10.1029/2012jb009205
- Buffett, B. A., & Heuret, A. (2011, jun). Curvature of subducted lithosphere from earthquake locations in the Wadati-Benioff zone. *Geochemistry Geophysics, Geosystems*, 12(6). Retrieved from <http://dx.doi.org/10.1029/2011gc003570> doi: 10.1029/2011gc003570
- Capitanio, F., Morra, G., & Goes, S. (2007, October). Dynamic models of downgoing plate-buoyancy driven subduction: Subduction motions and energy dissipation. *Earth and Planetary Science Letters*, 262(1-2), 284–297. Retrieved from <https://doi.org/10.1016/j.epsl.2007.07.039> doi: 10.1016/j.epsl.2007.07.039
- Capitanio, F. A., Morra, G., & Goes, S. (2009, April). Dynamics of plate bending at the trench and slab-plate coupling. *Geochemistry, Geophysics, Geosystems*, 10(4), n/a–n/a. Retrieved from <https://doi.org/10.1029/2008gc002348> doi: 10.1029/2008gc002348
- Chapple, W. M., & Forsyth, D. W. (1979, November). Earthquakes and bending of plates at trenches. *Journal of Geophysical Research: Solid Earth*, 84(B12), 6729–6749. Retrieved from <https://doi.org/10.1029/jb084ib12p06729> doi: 10.1029/jb084ib12p06729
- Chen, M., Manea, V. C., Niu, F., Wei, S. S., & Kiser, E. (2019, February). Genesis of intermediate-depth and deep intraslab earthquakes beneath Japan constrained by seismic tomography, seismicity, and thermal mod-

- eling. *Geophysical Research Letters*, 46(4), 2025–2036. Retrieved from
<https://doi.org/10.1029/2018gl080025> doi: 10.1029/2018gl080025
- Coblentz, D. D., Richardson, R. M., & Sandiford, M. (1994, August). On the gravitational potential of the earths lithosphere. *Tectonics*, 13(4), 929–945. Retrieved from <https://doi.org/10.1029/94tc01033> doi: 10.1029/94tc01033
- Comte, D., Dorbath, L., Pardo, M., Monfret, T., Haessler, H., Rivera, L., ... Meneses, C. (1999, July). A double-layered seismic zone in arica, northern chile. *Geophysical Research Letters*, 26(13), 1965–1968. Retrieved from <https://doi.org/10.1029/1999gl900447> doi: 10.1029/1999gl900447
- Comte, D., & Suarez, G. (1994, January). An inverted double seismic zone in chile: Evidence of phase transformation in the subducted slab. *Science*, 263(5144), 212–215. Retrieved from <https://doi.org/10.1126/science.263.5144.212> doi: 10.1126/science.263.5144.212
- Conrad, C. P., & Lithgow-Bertelloni, C. (2002, October). How mantle slabs drive plate tectonics. *Science*, 298(5591), 207–209. Retrieved from <https://doi.org/10.1126/science.1074161> doi: 10.1126/science.1074161
- Conrad, C. P., & Lithgow-Bertelloni, C. (2004, October). The temporal evolution of plate driving forces: Importance of “slab suction” versus “slab pull” during the cenozoic. *Journal of Geophysical Research: Solid Earth*, 109(B10). Retrieved from <https://doi.org/10.1029/2004jb002991> doi: 10.1029/2004jb002991
- Craig, T. J. (2019, February). Accurate depth determination for moderate-magnitude earthquakes using global teleseismic data. *Journal of Geophysical Research: Solid Earth*, 124(2), 1759–1780. Retrieved from <https://doi.org/10.1029/2018jb016902> doi: 10.1029/2018jb016902
- Craig, T. J., & Copley, A. (2018, February). Forearc collapse, plate flexure, and seismicity within the downgoing plate along the sunda arc west of sumatra. *Earth and Planetary Science Letters*, 484, 81–91. Retrieved from <https://doi.org/10.1016/j.epsl.2017.12.004> doi: 10.1016/j.epsl.2017.12.004
- Craig, T. J., Copley, A., & Jackson, J. (2014, February). A reassessment of outer-rise seismicity and its implications for the mechanics of oceanic lithosphere. *Geophysical Journal International*, 197(1), 63–89. Retrieved from <https://doi.org/10.1093/gji/ggu013> doi: 10.1093/gji/ggu013
- Ekström, G., Nettles, M., & Dziewoński, A. (2012, June). The global CMT project

- 1176 2004–2010: Centroid-moment tensors for 13, 017 earthquakes. *Physics of*
1177 *the Earth and Planetary Interiors, 200-201*, 1–9. Retrieved from <https://doi.org/10.1016/j.pepi.2012.04.002> doi: 10.1016/j.pepi.2012.04.002
- 1178 Elsasser, W. M. (1969). Convection and stress propagation in the upper mantle.
- 1180 Emmerson, B., & McKenzie, D. (2007, August). Thermal structure and seismicity of
1181 subducting lithosphere. *Physics of the Earth and Planetary Interiors, 163*(1–
1182 4), 191–208. Retrieved from <https://doi.org/10.1016/j.pepi.2007.05.007>
1183 doi: 10.1016/j.pepi.2007.05.007
- 1184 Engdahl, E. R., & Scholz, C. H. (1977, October). A double benioff zone beneath
1185 the central aleutians: An unbending of the lithosphere. *Geophysical Re-*
1186 *search Letters, 4*(10), 473–476. Retrieved from <https://doi.org/10.1029/gl004i010p00473> doi: 10.1029/gl004i010p00473
- 1188 Engdahl, E. R., van der Hilst, R., & Buland, R. (1998). Global teleseismic earth-
1189 quake relocation with improved travel times and procedures for depth determi-
1190 nation. *Bulletin of the Seismological Society of America, 88*(3), 722–743.
- 1191 England, P., & Wilkins, C. (2004, December). A simple analytical approximation to
1192 the temperature structure in subduction zones. *Geophysical Journal Interna-*
1193 *tional, 159*(3), 1138–1154. Retrieved from <https://doi.org/10.1111/j.1365-246x.2004.02419.x> doi: 10.1111/j.1365-246x.2004.02419.x
- 1195 Faccenda, M. (2014, February). Water in the slab: A trilogy. *Tectonophysics, 614*,
1196 1–30. Retrieved from <https://doi.org/10.1016/j.tecto.2013.12.020> doi:
1197 10.1016/j.tecto.2013.12.020
- 1198 Forsyth, D., & Uyeda, S. (1975, oct). On the relative importance of the driving
1199 forces of plate motion. *Geophysical Journal International, 43*(1), 163–200.
1200 Retrieved from <http://dx.doi.org/10.1111/j.1365-246x.1975.tb00631.x>
1201 doi: 10.1111/j.1365-246x.1975.tb00631.x
- 1202 Fuenzalida, A., Schurr, B., Lancieri, M., Sobiesiak, M., & Madariaga, R. (2013,
1203 May). High-resolution relocation and mechanism of aftershocks of the 2007
1204 tocopilla (chile) earthquake. *Geophysical Journal International, 194*(2),
1205 1216–1228. Retrieved from <https://doi.org/10.1093/gji/ggt163> doi:
1206 10.1093/gji/ggt163
- 1207 Fujita, K., & Kanamori, H. (1981a, July). Double seismic zones and stresses of in-
1208 termediate depth earthquakes. *Geophysical Journal International, 66*(1), 131–

- 1209 156. Retrieved from <https://doi.org/10.1111/j.1365-246x.1981.tb05950.x>
1210 .x doi: 10.1111/j.1365-246x.1981.tb05950.x
- 1211 Fujita, K., & Kanamori, H. (1981b, July). Double seismic zones and stresses of in-
1212 termediate depth earthquakes. *Geophysical Journal International*, 66(1), 131–
1213 156. Retrieved from <https://doi.org/10.1111/j.1365-246x.1981.tb05950.x>
1214 .x doi: 10.1111/j.1365-246x.1981.tb05950.x
- 1215 Gerardi, G., & Ribe, N. M. (2018, June). Boundary element modeling of two-plate
1216 interaction at subduction zones: Scaling laws and application to the aleu-
1217 tian subduction zone. *Journal of Geophysical Research: Solid Earth*, 123(6),
1218 5227–5248. Retrieved from <https://doi.org/10.1002/2017jb015148> doi:
1219 10.1002/2017jb015148
- 1220 Ghosh, A., Holt, W. E., & Flesch, L. M. (2009, November). Contribution of grav-
1221 itational potential energy differences to the global stress field. *Geophysical
1222 Journal International*, 179(2), 787–812. Retrieved from [https://doi.org/
1223 10.1111/j.1365-246x.2009.04326.x](https://doi.org/10.1111/j.1365-246x.2009.04326.x) doi: 10.1111/j.1365-246x.2009.04326.x
- 1224 Goes, S., Capitanio, F., Morra, G., Seton, M., & Giardini, D. (2011). Signatures
1225 of downgoing plate-buoyancy driven subduction in cenozoic plate motions.
- 1226 *Physics of the Earth and Planetary Interiors*, 184(1-2), 1–13. Retrieved from
1227 <https://doi.org/10.1016/j.pepi.2010.10.007>
- 1228 Green, H. W., & Houston, H. (1995). The mechanics of deep earthquakes. *Annual
1229 Review of Earth and Planetary Sciences*, 23(1), 169–213.
- 1230 Gurnis, M., Ritsema, J., Heijst, H.-J. V., & Zhong, S. (2000, August). Tonga slab
1231 deformation: The influence of a lower mantle upwelling on a slab in a young
1232 subduction zone. *Geophysical Research Letters*, 27(16), 2373–2376. Retrieved
1233 from <https://doi.org/10.1029/2000gl011420> doi: 10.1029/2000gl011420
- 1234 Gutenberg, B., & Richter, C. (1954). *Seismicity of the world and associated phenom-
1235 ena*. Princeton University Press, Princeton, NJ.
- 1236 Gutscher, M.-A., Spakman, W., Bijwaard, H., & Engdahl, E. R. (2000, Octo-
1237 ber). Geodynamics of flat subduction: Seismicity and tomographic con-
1238 straints from the andean margin. *Tectonics*, 19(5), 814–833. Retrieved from
1239 <https://doi.org/10.1029/1999tc001152> doi: 10.1029/1999tc001152
- 1240 Hacker, B. R., Peacock, S. M., Abers, G. A., & Holloway, S. D. (2003, January).
1241 Subduction factory 2. are intermediate-depth earthquakes in subducting slabs

- 1242 linked to metamorphic dehydration reactions? *Journal of Geophysical Re-*
 1243 *search: Solid Earth*, 108(B1). Retrieved from <https://doi.org/10.1029/2001jb001129> doi: 10.1029/2001jb001129
- 1244 Hasegawa, A., Umino, N., & Takagi, A. (1978, May). Double-planed structure of the
 1245 deep seismic zone in the northeastern japan arc. *Tectonophysics*, 47(1-2), 43–
 1246 58. Retrieved from [https://doi.org/10.1016/0040-1951\(78\)90150-6](https://doi.org/10.1016/0040-1951(78)90150-6) doi:
 1247 10.1016/0040-1951(78)90150-6
- 1248 Hayes, G. P., Moore, G. L., Portner, D. E., Hearne, M., Flamme, H., Furtney,
 1249 M., & Smoczyk, G. M. (2018, August). Slab2, a comprehensive subduc-
 1250 tion zone geometry model. *Science*, 362(6410), 58–61. Retrieved from
 1251 <https://doi.org/10.1126/science.aat4723> doi: 10.1126/science.aat4723
- 1252 Hayes, G. P., Wald, D. J., & Johnson, R. L. (2012, January). Slab1.0: A
 1253 three-dimensional model of global subduction zone geometries. *Journal
 1254 of Geophysical Research: Solid Earth*, 117(B1), n/a–n/a. Retrieved from
 1255 <https://doi.org/10.1029/2011jb008524> doi: 10.1029/2011jb008524
- 1256 House, L. S., & Jacob, K. H. (1982, February). Thermal stresses in subducting litho-
 1257 sphere can explain double seismic zones. *Nature*, 295(5850), 587–589. Re-
 1258 trieval from <https://doi.org/10.1038/295587a0> doi: 10.1038/295587a0
- 1259 Hunter, J., & Watts, A. (2016, July). Gravity anomalies, flexure and mantle rhe-
 1260 ology seaward of circum-pacific trenches. *Geophysical Journal International*,
 1261 207(1), 288–316. Retrieved from <https://doi.org/10.1093/gji/ggw275> doi:
 1262 10.1093/gji/ggw275
- 1263 Imanishi, K., Ando, R., & Kuwahara, Y. (2012, May). Unusual shallow normal-
 1264 faulting earthquake sequence in compressional northeast japan activated
 1265 after the 2011 off the pacific coast of tohoku earthquake. *Geophysical Re-*
 1266 *search Letters*, 39(9), n/a–n/a. Retrieved from <https://doi.org/10.1029/2012gl051491> doi: 10.1029/2012gl051491
- 1267 Isacks, B., & Barazangi, M. (1977). Geometry of benioff zones: Lateral segmen-
 1268 tation and downwards bending of the subducted lithosphere. In *Island arcs,
 1269 deep sea trenches and back-arc basins* (pp. 99–114). American Geophysi-
 1270 cal Union. Retrieved from <https://doi.org/10.1029/me001p0099> doi:
 1271 10.1029/me001p0099
- 1272 Isacks, B., & Molnar, P. (1969, sep). Mantle Earthquake Mechanisms and the Sink-
 1273

- 1275 ing of the Lithosphere. *Nature*, 223(5211), 1121–1124. Retrieved from <http://dx.doi.org/10.1038/2231121a0> doi: 10.1038/2231121a0
- 1276
- 1277 Isacks, B., & Molnar, P. (1971). Distribution of stresses in the descending litho-
1278 sphere from a global survey of focal-mechanism solutions of mantle earth-
1279 quakes. *Review of Geophysics*, 9(1), 103. Retrieved from <http://dx.doi.org/10.1029/rg009i001p00103> doi: 10.1029/rg009i001p00103
- 1280
- 1281 Jackson, J. (1980, May). Errors in focal depth determination and the depth of
1282 seismicity in iran and turkey. *Geophysical Journal International*, 61(2), 285–
1283 301. Retrieved from <https://doi.org/10.1111/j.1365-246x.1980.tb04318.x>
1284 doi: 10.1111/j.1365-246x.1980.tb04318.x
- 1285
- 1286 Kawakatsu, H. (1986a). Double seismic zones: Kinematics. *Journal of Geo-
1287 physical Research*, 91(B5), 4811. Retrieved from <https://doi.org/10.1029/jb091ib05p04811> doi: 10.1029/jb091ib05p04811
- 1288
- 1289 Kawakatsu, H. (1986b). Downdip tensional earthquakes beneath the tonga
1290 arc: A double seismic zone? *Journal of Geophysical Research*, 91(B6),
1291 6432. Retrieved from <https://doi.org/10.1029/jb091ib06p06432> doi:
10.1029/jb091ib06p06432
- 1292
- 1293 Kirby, S., Engdahl, R. E., & Denlinger, R. (2013, March). Intermediate-depth
1294 intraslab earthquakes and arc volcanism as physical expressions of crustal
and uppermost mantle metamorphism in subducting slabs. In *Subduction
1295 top to bottom* (pp. 195–214). American Geophysical Union. Retrieved from
1296 <https://doi.org/10.1029/gm096p0195> doi: 10.1029/gm096p0195
- 1297
- 1298 Kita, S., Okada, T., Hasegawa, A., Nakajima, J., & Matsuzawa, T. (2010, De-
1299 cember). Existence of interplane earthquakes and neutral stress boundary
1300 between the upper and lower planes of the double seismic zone beneath to-
hoku and hokkaido, northeastern japan. *Tectonophysics*, 496(1-4), 68–82.
1301 Retrieved from <https://doi.org/10.1016/j.tecto.2010.10.010> doi:
1302 10.1016/j.tecto.2010.10.010
- 1303
- 1304 Lemoine, A., Madariaga, R., & Campos, J. (2002, September). Slab-pull and
1305 slab-push earthquakes in the mexican, chilean and peruvian subduction
1306 zones. *Physics of the Earth and Planetary Interiors*, 132(1-3), 157–175.
1307 Retrieved from [https://doi.org/10.1016/s0031-9201\(02\)00050-x](https://doi.org/10.1016/s0031-9201(02)00050-x) doi:
10.1016/s0031-9201(02)00050-x

- 1308 Lister, G., Kennett, B., Richards, S., & Forster, M. (2008). Boudinage of a stretch-
 1309 ing slablet implicated in earthquakes beneath the hindu kush. *Nature Geo-*
 1310 *science*, 1(3), 196.
- 1311 Lorinczi, P., & Houseman, G. (2009, September). Lithospheric gravitational instabil-
 1312 ity beneath the southeast carpathians. *Tectonophysics*, 474(1-2), 322–336. Re-
 1313 tried from <https://doi.org/10.1016/j.tecto.2008.05.024> doi: 10.1016/
 1314 j.tecto.2008.05.024
- 1315 Manea, V., & Gurnis, M. (2007, December). Subduction zone evolution and low
 1316 viscosity wedges and channels. *Earth and Planetary Science Letters*, 264(1-2),
 1317 22–45. Retrieved from <https://doi.org/10.1016/j.epsl.2007.08.030> doi:
 1318 10.1016/j.epsl.2007.08.030
- 1319 McAdoo, D. C., Caldwell, J. G., & Turcotte, D. L. (1978, July). On the elastic-
 1320 perfectly plastic bending of the lithosphere under generalized loading with
 1321 application to the kuril trench. *Geophysical Journal International*, 54(1), 11–
 1322 26. Retrieved from <https://doi.org/10.1111/j.1365-246x.1978.tb06753.x>
 1323 doi: 10.1111/j.1365-246x.1978.tb06753.x
- 1324 McCrory, P. A., Blair, J. L., Waldhauser, F., & Oppenheimer, D. H. (2012, Septem-
 1325 ber). Juan de fuca slab geometry and its relation to wadati-benioff zone seis-
 1326 micity. *Journal of Geophysical Research: Solid Earth*, 117(B9). Retrieved from
 1327 <https://doi.org/10.1029/2012jb009407> doi: 10.1029/2012jb009407
- 1328 McKenzie, D. P. (1969, September). Speculations on the consequences and causes of
 1329 plate motions. *Geophysical Journal International*, 18(1), 1–32. Retrieved
 1330 from <https://doi.org/10.1111/j.1365-246x.1969.tb00259.x> doi:
 1331 10.1111/j.1365-246x.1969.tb00259.x
- 1332 Molnar, P., & Bendick, R. (2019, May). Seismic moments of intermediate-
 1333 depth earthquakes beneath the hindu kush: Active stretching of a blob
 1334 of sinking thickened mantle lithosphere? *Tectonics*. Retrieved from
 1335 <https://doi.org/10.1029/2018tc005336> doi: 10.1029/2018tc005336
- 1336 Nothard, S., McKenzie, D., Haines, J., & Jackson, J. (1996, November). Gaussian
 1337 curvature and the relationship between the shape and the deformation
 1338 of the tonga slab. *Geophysical Journal International*, 127(2), 311–327. Re-
 1339 tried from <https://doi.org/10.1111/j.1365-246x.1996.tb04722.x> doi:
 1340 10.1111/j.1365-246x.1996.tb04722.x

- 1341 Peacock, S. M. (2001). Are the lower planes of double seismic zones caused by
1342 serpentine dehydration in subducting oceanic mantle? *Geology*, 29(4), 299.
1343 Retrieved from [https://doi.org/10.1130/0091-7613\(2001\)029<0299:atlpod>2.0.co;2](https://doi.org/10.1130/0091-7613(2001)029<0299:atlpod>2.0.co;2)
1344 doi: 10.1130/0091-7613(2001)029<0299:atlpod>2.0.co;2
- 1345 Ribe, N. M. (2001, apr). Bending and stretching of thin viscous sheets. *Journal of*
1346 *Fluid Mechanics*, 433, 135–160. Retrieved from <http://dx.doi.org/10.1017/s0022112000003360> doi: 10.1017/s0022112000003360
- 1348 Ribe, N. M. (2010, feb). Bending mechanics and mode selection in free subduction:
1349 a thin-sheet analysis. *Geophysical Journal International*, 180(2), 559–576. Re-
1350 trieval from <http://dx.doi.org/10.1111/j.1365-246x.2009.04460.x> doi:
1351 10.1111/j.1365-246x.2009.04460.x
- 1352 Richter, F. M. (1979, November). Focal mechanisms and seismic energy release
1353 of deep and intermediate earthquakes in the tonga-kermadec region and their
1354 bearing on the depth extent of mantle flow. *Journal of Geophysical Research: Solid*
1355 *Earth*, 84(B12), 6783–6795. Retrieved from <https://doi.org/10.1029/jb084ib12p06783> doi: 10.1029/jb084ib12p06783
- 1357 Rietbrock, A., & Waldhauser, F. (2004, May). A narrowly spaced double-seismic
1358 zone in the subducting nazca plate. *Geophysical Research Letters*, 31(10), n/a–
1359 n/a. Retrieved from <https://doi.org/10.1029/2004gl019610> doi: 10.1029/
1360 2004gl019610
- 1361 Romeo, I., & Álvarez-Gómez, J. (2018). Lithospheric folding by flexural slip in sub-
1362 duction zones as source for reverse fault intraslab earthquakes. *Scientific re-*
1363 *ports*, 8(1), 1367.
- 1364 Samowitz, I. R., & Forsyth, D. W. (1981). Double seismic zone beneath the
1365 mariana island arc. *Journal of Geophysical Research*, 86(B8), 7013. Re-
1366 trieval from <https://doi.org/10.1029/jb086ib08p07013> doi: 10.1029/
1367 jb086ib08p07013
- 1368 Sandiford, D., & Moresi, L. (2019, June). Improving subduction interface imple-
1369 mentation in dynamic numerical models. *Solid Earth*, 10(3), 969–985. Re-
1370 trieval from <https://doi.org/10.5194/se-10-969-2019> doi: 10.5194/se-10
1371 -969-2019
- 1372 Sandiford, D., Moresi, L., Sandiford, M., & Yang, T. (2019, December). Geometric
1373 controls on flat slab seismicity. *Earth and Planetary Science Letters*, 527,

- 1374 115787. Retrieved from <https://doi.org/10.1016/j.epsl.2019.115787>
1375 doi: 10.1016/j.epsl.2019.115787
- 1376 Sandiford, M., Coblenz, D., & Schellart, W. P. (2005). Evaluating slab-plate
1377 coupling in the indo-australian plate. *Geology*, 33(2), 113. Retrieved from
1378 <https://doi.org/10.1130/g20898.1> doi: 10.1130/g20898.1
- 1379 Schellart, W. (2017). Andean mountain building and magmatic arc migration driven
1380 by subduction-induced whole mantle flow. *Nature communications*, 8(1),
1381 2010.
- 1382 Schellart, W. P. (2004, April). Quantifying the net slab pull force as a driv-
1383 ing mechanism for plate tectonics. *Geophysical Research Letters*, 31(7),
1384 n/a–n/a. Retrieved from <https://doi.org/10.1029/2004gl019528> doi:
1385 10.1029/2004gl019528
- 1386 Seno, T., & Yamanaka, Y. (2013, March). Double seismic zones, compressional
1387 deep trench-outer rise events, and superplumes. In *Subduction top to bottom*
1388 (pp. 347–355). American Geophysical Union. Retrieved from <https://doi.org/10.1029/gm096p0347> doi: 10.1029/gm096p0347
- 1390 Shillington, D. J., Bécel, A., Nedimović, M. R., Kuehn, H., Webb, S. C., Abers,
1391 G. A., ... Mattei-Salicrup, G. A. (2015). Link between plate fabric, hydration
1392 and subduction zone seismicity in alaska. *Nature Geoscience*, 8(12), 961.
- 1393 Sippl, C., Schurr, B., Asch, G., & Kummerow, J. (2018, May). Seismicity struc-
1394 ture of the northern chile forearc from 100, 000 double-difference relocated
1395 hypocenters. *Journal of Geophysical Research: Solid Earth*, 123(5), 4063–
1396 4087. Retrieved from <https://doi.org/10.1002/2017jb015384> doi:
1397 10.1002/2017jb015384
- 1398 Sleep, N. H. (1979). The double seismic zone in downgoing slabs and the
1399 viscosity of the mesosphere. *Journal of Geophysical Research*, 84(B9),
1400 4565. Retrieved from <https://doi.org/10.1029/jb084ib09p04565> doi:
1401 10.1029/jb084ib09p04565
- 1402 Sleep, N. H. (2012). Constraint on the recurrence of great outer-rise earthquakes
1403 from seafloor bathymetry. *Earth, Planets and Space*, 64(12), 19.
- 1404 Tsujimori, T., Sisson, V., Liou, J., Harlow, G., & Sorensen, S. (2006, December).
1405 Very-low-temperature record of the subduction process: A review of world-
1406 wide lawsonite eclogites. *Lithos*, 92(3-4), 609–624. Retrieved from <https://doi.org/10.1016/j.lithos.2006.09.001> doi: 10.1016/j.lithos.2006.09.001

- 1407 doi.org/10.1016/j.lithos.2006.03.054 doi: 10.1016/j.lithos.2006.03.054
- 1408 Tsukahara, H. (1980). Physical conditions for double seismic planes of the deep seis-
1409 mic zone. *Journal of Physics of the Earth*, 28(1), 1–15.
- 1410 Turcotte, D., McAdoo, D., & Caldwell, J. (1978, June). An elastic-perfectly plastic
1411 analysis of the bending of the lithosphere at a trench. *Tectonophysics*, 47(3-4),
1412 193–205. Retrieved from [https://doi.org/10.1016/0040-1951\(78\)90030-6](https://doi.org/10.1016/0040-1951(78)90030-6)
1413 doi: 10.1016/0040-1951(78)90030-6
- 1414 van Hunen, J., van den Berg, A. P., & Vlaar, N. J. (2004, August). Various mech-
1415 anisms to induce present-day shallow flat subduction and implications for the
1416 younger earth: a numerical parameter study. *Physics of the Earth and Plane-*
1417 *tary Interiors*, 146(1-2), 179–194. Retrieved from <https://doi.org/10.1016/j.pepi.2003.07.027>
1418 doi: 10.1016/j.pepi.2003.07.027
- 1419 van Summeren, J., Conrad, C. P., & Lithgow-Bertelloni, C. (2012, February). The
1420 importance of slab pull and a global asthenosphere to plate motions. *Geochem-*
1421 *istry, Geophysics, Geosystems*, 13(2), n/a–n/a. Retrieved from <https://doi.org/10.1029/2011gc003873>
1422 doi: 10.1029/2011gc003873
- 1423 Vassiliou, M., Hager, B., & Raefsky, A. (1984, February). The distribution of
1424 earthquakes with depth and stress in subducting slabs. *Journal of Geo-*
1425 *dynamics*, 1(1), 11–28. Retrieved from [https://doi.org/10.1016/0264-3707\(84\)90004-8](https://doi.org/10.1016/0264-3707(84)90004-8)
1426 doi: 10.1016/0264-3707(84)90004-8
- 1427 Wagner, L. S., & Okal, E. A. (2019, July). The pucallpa nest and its constraints on
1428 the geometry of the peruvian flat slab. *Tectonophysics*, 762, 97–108. Retrieved
1429 from <https://doi.org/10.1016/j.tecto.2019.04.021> doi: 10.1016/j.tecto
1430 .2019.04.021
- 1431 Wang, K. (2002, September). Unbending combined with dehydration embrittlement
1432 as a cause for double and triple seismic zones. *Geophysical Research Letters*,
1433 29(18), 36–1–36–4. Retrieved from <https://doi.org/10.1029/2002gl015441>
1434 doi: 10.1029/2002gl015441
- 1435 Yang, T., Gurnis, M., & Zhan, Z. (2017, July). Trench motion-controlled slab mor-
1436 phology and stress variations: Implications for the isolated 2015 bonin islands
1437 deep earthquake. *Geophysical Research Letters*, 44(13), 6641–6650. Retrieved
1438 from <https://doi.org/10.1002/2017gl073989> doi: 10.1002/2017gl073989
- 1439 Yang, T., Moresi, L., Gurnis, M., Liu, S., Sandiford, D., Williams, S., & Capi-

1440 tanio, F. A. (2019, July). Contrasted east asia and south america tectonics
1441 driven by deep mantle flow. *Earth and Planetary Science Letters*, 517, 106–
1442 116. Retrieved from <https://doi.org/10.1016/j.epsl.2019.04.025> doi:
1443 10.1016/j.epsl.2019.04.025